AFRL-RX-WP-TP-2008-4323

PRECIPITATION OF $Al_3(Sc,Zr)$ PARTICLES IN A DIRECT CHILL CAST Al-Zn-Mg-Cu-Sc-Zr ALLOY DURING CONVENTIONAL SOLUTION HEAT TREATMENT AND ITS EFFECT ON TENSILE PROPERTIES (PREPRINT)

O.N. Senkov, M.R. Shaghiev, S.V. Senkova, and D.B. Miracle

UES, Inc.

DECEMBER 2007

AIR FORCE RESEARCH LABORATORY
MATERIALS AND MANUFACTURING DIRECTORATE
WRIGHT-PATTERSON AIR FORCE BASE, OH 45433-7750
AIR FORCE MATERIEL COMMAND
UNITED STATES AIR FORCE

REPORT DOCUMENTATION PAGE

Form Approved
OMB No. 0704-0188

1. REPORT DATE *(DD-MM-YY)*	2. REPORT TYPE	3. DATES COVERED *(From - To)*
December 2007	Journal Article Preprint	

4. TITLE AND SUBTITLE

PRECIPITATION OF $Al_3(Sc,Zr)$ PARTICLES IN A DIRECT CHILL CAST Al-Zn-Mg-Cu-Sc-Zr ALLOY DURING CONVENTIONAL SOLUTION HEAT TREATMENT AND ITS EFFECT ON TENSILE PROPERTIES (PREPRINT)

5a. CONTRACT NUMBER
FA8650-04-D-5233

5b. GRANT NUMBER

5c. PROGRAM ELEMENT NUMBER
62102F

6. AUTHOR(S)

O.N. Senkov, M.R. Shaghiev, and S.V. Senkova (UES, Inc.)
D.B. Miracle (AFRL/RXLMP)

5d. PROJECT NUMBER
2311

5e. TASK NUMBER
00

5f. WORK UNIT NUMBER
23110002

7. PERFORMING ORGANIZATION NAME(S) AND ADDRESS(ES)

UES, Inc.
4401 Dayton-Xenia Road
Dayton OH 45432-1894

Metals Branch (AFRL/RXLM)
Metals, Ceramics, and NDE Division
Materials and Manufacturing Directorate
Wright-Patterson Air Force Base, OH 45433-7750
Air Force Materiel Command, United States Air Force

8. PERFORMING ORGANIZATION REPORT NUMBER

9. SPONSORING/MONITORING AGENCY NAME(S) AND ADDRESS(ES)

Air Force Research Laboratory
Materials and Manufacturing Directorate
Wright-Patterson Air Force Base, OH 45433-7750
Air Force Materiel Command
United States Air Force

10. SPONSORING/MONITORING AGENCY ACRONYM(S)
AFRL/RXLM

11. SPONSORING/MONITORING AGENCY REPORT NUMBER(S)
AFRL-RX-WP-TP-2008-4323

12. DISTRIBUTION/AVAILABILITY STATEMENT
Approved for public release; distribution unlimited.

13. SUPPLEMENTARY NOTES
Journal article submitted to *Acta Materialia*. PAO Case Number: WPAFB 07-0536; Clearance Date: 26 Nov 2007. The U.S. Government is joint author of this work and has the right to use, modify, reproduce, release, perform, display, or disclose the work.

14. ABSTRACT

The effect of heat treatment on precipitation and growth of coherent nanometer-sized $Al_3(Sc,Zr)$ particles and the effect of these particles on tensile properties of a direct chill (DC) cast Al-Zn-Mg- Cu-Sc-Zr alloy were studied. The size distribution, average size, number density and volume fraction of the $Al_3(Sc,Zr)$ particles were determined as a function of the solution treatment temperature and time. The average particle diameter increased from 6.0 nm to 27.3 nm, the volume fraction increased from 0.11% to 0.46%, while their number density decreased from 5.4×10^{15} cm-3 to 3.1×10^{14} cm^{-3} with an increase in the solution treatment temperature from 460°C to 480°C and holding time from 1 hour to 48 hours. The particle size distributions were well described by normal (Gaussian) distributions but did not follow the Lifshitz-Slyozov-Wagner (LSW) theory of Ostwald ripening. To describe the observed particle size distributions, a stochastic process of particle growth was added to the normal process of growth. The kinetics of phase transformation followed the Kolmogorov- Johnson-Mehl-Avrami (KJMA) law, with the Avrami exponent $m = 0.404$.

15. SUBJECT TERMS
aluminum alloy, tensile properties, Lifshitz-Slyozov-Wagner theory, Kolmogorov-Johnson-Mehl-Avrami law, direct chill, tensile strength

16. SECURITY CLASSIFICATION OF:			17. LIMITATION OF ABSTRACT:	18. NUMBER OF PAGES	19a. NAME OF RESPONSIBLE PERSON (Monitor)
a. REPORT	b. ABSTRACT	c. THIS PAGE			John H. Barnes
Unclassified	Unclassified	Unclassified	SAR	52	19b. TELEPHONE NUMBER *(Include Area Code)* N/A

Standard Form 298 (Rev. 8-98)
Prescribed by ANSI Std. Z39-18

Precipitation of $Al_3(Sc,Zr)$ Particles in a Direct Chill Cast Al-Zn-Mg-Cu-Sc-Zr Alloy During Conventional Solution Heat Treatment and Its Effect on Tensile Properties

O.N. Senkov[1*], M.R. Shaghiev[1†], S.V. Senkova[1], D.B. Miracle

Air Force Research Laboratory, Materials and Manufacturing Directorate, Wright-Patterson AFB, Ohio 45433-7817.

[1] UES, Inc., 4401 Dayton-Xenia Rd., Dayton, Ohio, 45432-1894

ABSTRACT

The effect of heat treatment on precipitation and growth of coherent nanometer-sized $Al_3(Sc,Zr)$ particles and the effect of these particles on tensile properties of a direct chill (DC) cast Al-Zn-Mg-Cu-Sc-Zr alloy were studied. The size distribution, average size, number density and volume fraction of the $Al_3(Sc,Zr)$ particles were determined as a function of the solution treatment temperature and time. The average particle diameter increased from 6.0 nm to 27.3 nm, the volume fraction increased from 0.11% to 0.46%, while their number density decreased from 5.4×10^{15} cm^{-3} to 3.1×10^{14} cm^{-3} with an increase in the solution treatment temperature from 460°C to 480°C and holding time from 1 hour to 48 hours. The particle size distributions were well described by normal (Gaussian) distributions but did not follow the Lifshitz-Slyozov-Wagner (LSW) theory of Ostwald ripening. To describe the observed particle size distributions, a stochastic process of particle growth was added to the normal process of growth. The kinetics of phase transformation followed the Kolmogorov-Johnson-Mehl-Avrami (KJMA) law, with the Avrami exponent m = 0.404. Room temperature mechanical properties were evaluated in the as-solution treated condition and after aging at 120°C for 19 hours. In the as-solution treated condition, the highest values of the yield strength of 331 MPa and the ultimate strength of 503 MPa corresponded to the alloy with the smallest $Al_3(Sc,Zr)$ particle size of 6.0 nm. Aging at 120°C for 19 hours led to precipitation of GPII zones and η' particles, which considerably increased the tensile strength (YS ≈ 530 MPa, UTS ≈ 610 MPa); however, the relative strengthening effect from the $Al_3(Sc,Zr)$ particles was reduced.

---

[*] Corresponding author. E-mail address: oleg.senkov@wpafb.af.mil; Phone: 937-2551320; Fax: 937-6567292.

[†] Currently at the Institute for Metals Superplasticity Problems, Ufa, Russia.

,INTRODUCTION

Aerospace industry has a substantial interest to new low-cost materials with improved specific strengths and resistance to fracture. 7000 series Al-Zn-Mg-Cu alloys possess the highest strength among all commercial Al alloys [1]. However these alloys generally have poor ductility and low fracture strength in the as-cast condition, and extensive processing, which includes combination of heat treatment and hot working, is required to improve the mechanical properties [2]. Fortunately, the fracture-related properties of these alloys can be considerably improved by small additions of Sc and Zr, which enable a superior combination of higher strength levels and acceptable ductility, in both cast and wrought conditions [3,4,5,6,7,8,9,10]. Starting from refining the grain size of the cast aluminum alloys, additions of Sc and Zr also increase the resistance to recrystallization during hot working and introduce additional strengthening through the formation of fine coherent $Al_3(Sc,Zr)$ particles from a super-saturated solid solution [8,9,10]. Homogeneous distribution of these particles promotes formation of a stable refined subgrain structure during deformation processing, which adds an additional increase in strength [6]. Accordingly, the maximum benefit of additions of Sc and Zr is obtained by producing a supersaturated solid solution of these elements after casting which is then decomposed to produce a high number density of the secondary $Al_3(Sc,Zr)$ particles during controlled heat treatment [11]. Because of low equilibrium solubility of Sc and Zr in the aluminum matrix, these particles precipitate from a supersaturated solid solution during first heat treatment after casting and cannot be dissolved after that, while the strengthening effect depends on their size and number density. Therefore, it is necessary to control precipitation of the $Al_3(Sc,Zr)$ particles, in order to achieve the best balance of mechanical properties. In the present work, kinetics of precipitation and growth of the secondary $Al_3(Sc,Zr)$ particles was studied during homogenization/solution treatment of a direct chill (DC) cast 7000 series alloy.

EXPERIMENTAL

A developmental 7000 series aluminum alloy, designated as SSA018 herein, with the chemical composition shown in Table 1 was produced by semi-continuous DC casting in the form of a 76 mm diameter billet. Specimens for microstructural analysis and tensile testing were extracted

from a billet region, which was located near the mid-radius of the billet. Flat tensile specimens had the gauge dimensions of 20×3.6×2.5 mm^3 and the longitudinal orientation, i.e. the specimen main axis was parallel to the billet's axis. The microstructure and tensile properties were studied in as-solution treated and aged conditions. Solution treatment was performed in air using a resistance heated box furnace with forced air convection. Different solution treatment temperatures (460ºC and 480ºC), heating rates (20°C/h and 60°C/h) and soaking times (1, 4, 20, and 48 hours) were selected. After ST and water quenching, several specimens were subjected to artificial aging at 120ºC for 19 hours.

Microstructural analysis was performed using transmission electron microscope (TEM) Phillips CM200 operating at an accelerating voltage of 200 kV. Thin foils for TEM were twin-jet electropolished at -30°C in a solution consisting of 20% HNO_3 and 80% CH_3OH. The sizes (diameters) and the number density of the $Al_3(Sc,Zr)$ particles were determined from several dark field (DF) TEM images taken at magnifications of 38,000X - 150,000X. These images were processed using Adobe Photoshop SC2 and then analyzed using Clemex Vision Pro 3.5 image processing software. From 1000 to 16000 particles were analyzed for every heat treatment condition (the number of counts increased with an increase in the particle number density).

Mechanical tensile tests were conducted at room temperature (RT, ~25ºC) using a servo-hydraulic MTS testing machine and a constant ram speed of 0.02 mm/s (initial strain rate was 10^{-3} s^{-1}). Two to three specimens per condition were tested.

RESULTS

Microstructural Analysis

In as-cast condition, the SSA018 alloy billet had a homogeneous equiaxed dendritic structure with the average grain size of 120 μm. This microstructure was described in detail elsewhere [8]. TEM analysis of the as-cast alloy revealed large eutectic-forming particles, which were enriched with Zn, Mg and Cu, and a dislocation network formed probably due to the internal stress relaxation during casting (Figure 1). No secondary $Al_3(Sc,Zr)$ particles were detected in this condition, which indicates that both Sc and Zr were in a super-saturated solid solution.

After solution treatment followed by water quenching, fine spherical $Al_3(Sc,Zr)$ particles formed (Figures 2, 3 and 4). The presence of the Ashby-Brown contrast on the bright-field images of

these particles, as well as the common locations of the $(h,k,l)_{Al}$ and $(2h,2k,2l)_{L12}$ electron diffraction spots, confirmed that the particles were coherent with the Al matrix. The size distributions of these $Al_3(Sc,Zr)$ particles after different heat treatment conditions are shown in Figure 5. The distributions are rather symmetrical relative to the mean particle size and they become wider with an increase in the solution treatment temperature and time. The size distributions can be well described by a normal distribution function $\Phi(d,t)$:

$$\Phi(d,t) = C\exp\left(\frac{(d-d_m)^2}{2\sigma^2}\right) \quad (1)$$

where d is the particle size (diameter), d_m is the mean size, σ is the standard deviation and C is a normalizing parameter. The entities d_m, σ and C are time dependent and their values are given in Table 2.

The mean size and the volume fraction of the $Al_3(Sc,Zr)$ particles increased and their number density decreased with an increase in the solution treatment time (Table 2). For example, after heating to 480°C with the heating rate of 20°C/h, holding at that temperature for 1 hour and subsequent water quenching, the mean diameter of the $Al_3(Sc,Zr)$ particles was 7.9 nm, the volume fraction was 0.16% and the number density was about 4.3×10^{15} cm^{-3}. An increase in the holding time at 480°C from 1 hour to 48 hours resulted in considerable coarsening, increasing volume fraction, and decreasing the number density (see also Figures 2a through 2d). After 48-hour solution treatment, the particles had the mean diameter of 27.3 nm, volume fraction of 0.42% and the number density of 1.9×10^{14} cm^{-3} (Figure 2d).

An increase in the heating rate from 20°C/h to 60°C/h prior to the solution treatment at 480°C, led to a slight decrease in the $Al_3(Sc,Zr)$ particle size and to an increase in their number density (see Table 2). For example, after 1-hour solution treatment, the mean diameter of the particles was 7.4 nm and their number density was about 4.4×10^{15} cm^{-3} (Figure 3a). After holding at 480°C for 48 hours, the mean diameter increased to 25.2 nm and their number density decreases to 4.2×10^{14} cm^{-3} (Figure 3d). The volume fraction of the particles increased from 0.17% to 0.46% with an increase in the solution treatment time in this case.

A decrease in the ST temperature from 480ºC to 460°C (at the same heating rate of 60°C/h) provided precipitation of the $Al_3(Sc,Zr)$ dispersoids with the smaller diameter and higher number density (compare Figures 3 and 4). For example, after 1-hour solution treatment at 460°C, the mean diameter of the particles was only 6.0 nm and the number density was about 5.4×10^{15} cm^{-3} (Figure 4a). Holding at 460ºC for 48 hours resulted in the $Al_3(Sc,Zr)$ particles with the mean size of 14.6 nm and the number density of 1.3×10^{15} cm^{-3} (Figure 4d). The volume fraction of the particles after holding for the same period of time was considerably lower at 460ºC than at 480ºC, which might indicate that some amounts of Sc and Zr were still present in a super-saturated solid solution, even after 48-hour holding at 460ºC.

Figure 6 shows dependencies of the mean $Al_3(Sc,Zr)$ particle size on the holding time during various solution treatments. The trend lines for these dependencies can be described by a power law equation:

$$d_m = At^B, \qquad (2)$$

where t is the holding time at a temperature, and A and B are constants which values depend on the heating rate and the solution treatment temperature. The A and B values are tabulated in Table 3. The value of the time exponent B is about 0.31 at 480ºC and 0.25 at 460ºC.

The surface area fraction, f_A, of the $Al_3(Sc,Zr)$ particles was also determined after different solution treatment conditions, and the values are given in Table 2 and they are also plotted versus the solution treatment time in Figure 7. It can be seen that the surface area fraction of these particles continuously increases with time at 460°C; however, f_A approaches maximum after annealing for about 4 hours and then decreases with an increase in the annealing time at 480°C.

Room temperature tensile properties after different heat treatments

Tensile properties of the DC cast SSA018 alloy were determined after solution treatment and natural aging for 24 hours (W24 temper) and after solution treatment and artificial aging at 120ºC for 19 hours (T6 temper). The results are given in Table 4. In the naturally aged specimens, both yield stress (YS) and ultimate tensile strength (UTS) decrease with an increase in the holding time at a solution treatment temperature. This decrease in the strength values can

be explained by coarsening of the $Al_3(Sc,Zr)$ particles during solution treatment. Indeed, Figure 8a shows that (a) both the YS and UTS continuously decrease with a decrease in the particle size and (b) the solution treatment conditions that provide the same $Al_3(Sc,Zr)$ particle size also provide the same strength values. The minimum particle size of 6.0 nm, which was achieved after the 60-460-1 solution treatment, provides the maximum values of YS = 331 MPa and UTS = 503 MPa. An increase in the mean particle size to 27.3 nm (after 20-480-48 solution treatment) decreases the YS and UTS by ~65 MPa and ~40 MPa, respectively, to YS = 267 MPa and UTS = 465 MPa.

Artificial aging at 120ºC for 19 hours followed after solution treatment and water quenching leads to an additional dramatic increase in both YS and UTS (see Figure 8b and Table 4), which is due to precipitation of *GP II* zones and η' particles [12,13]. The relative effect from the $Al_3(Sc,Zr)$ particles on the tensile strengths becomes much weaker, while the solution treatment conditions themselves become more important. Indeed, Figure 8b shows that while the tendency for YS and UTS to decrease with an increase in the $Al_3(Sc,Zr)$ particle size is still present after the T6 temper, the data points are much more scattered and, at the same solution treatment time, the specimens, which were solution treated at 480ºC, have higher YS and UTS values than those, which were solution treated at 460ºC. It can also be noticed that the 20-480 solution treated and T6 tempered specimens showed the maximum strength after 1 hour solution treatment, while the 60-480 and 60-460 solution treated and T6 tempered specimens showed the maximum strength values after 4 hours solution treatment. Probably, longer solution treatment time is required for the faster heated specimens to achieve maximum dissolution of the precipitate-forming elements (Zn, Mg, and Cu) at these solution treatment temperatures.

DISCUSSION

PRECIPITATION AND GROWTH OF SECONDARY $Al_3(Sc,Zr)$ PARTICLES IN THE SSA018 ALLOY

The results of the present work show that after DC casting of the SSA018 alloy, all Sc and Zr are present in the supersaturated solid solution and they precipitate into fine coherent nanometer-sized $Al_3(Sc,Zr)$ particles during conventional solution treatment (for Zn, Mg, and Cu) followed after the casting. The solution treatment consisted of continuous heating of the alloy from room

temperature to 460°C or 480°C with a heating rate of 20°C/h (5.56×10^{-3} K/s) or 60°C/h (1.67×10^{-2} K/s) and holding at the temperature for up to 48 hours and it is likely that the particles start to precipitate during the heating cycle. During holding at both 460°C and 480°C, the mean size and the volume fraction of the $Al_3(Sc,Zr)$ particles increase; however, the particle number density decreases and the particle/matrix interface area fraction go through a maximum with an increase in the solution treatment time. The increase in the volume fraction of these particles indicates that the precipitation continues during all period of the solution treatment, i.e. solubility of Sc and Zr in the Al matrix remains non-equilibrium. A simultaneous increase in the volume fraction and a decrease in the number density of the $Al_3(Sc,Zr)$ particles with an increase in the solution treatment time suggest that no new particles are formed during the treatment and their volume fraction increase is due to precipitation of Sc and Zr at the surfaces of already formed $Al_3(Sc,Zr)$ particles. In other words, the observed growth of the $Al_3(Sc,Zr)$ particles during solution treatment is probably due to simultaneous Sc and Zr precipitation at the particle/matrix interfaces and the particle coarsening.

It has recently been reported [14,15,16] that during heating of Al-Sc-Zr alloys precipitation of Sc and Zr from a supersaturated solid solution starts at about 250°C by formation of Al_3Sc clusters (due to faster diffusion of Sc in Al), and at temperatures above about 400°C, both Sc and Zr precipitate on already formed particles so that no new particles are formed at that time. It is expected that similar situation takes place in the SSA018 alloy studied in the present work, i.e. nucleation of the $Al_3(Sc,Zr)$ particles occurred during continuous heating to the solution treatment temperature, while growth and coarsening of these particles occurred during following holding at this temperature. As the volume fraction of the $Al_3(Sc,Zr)$ particles increases, the concentrations of Sc and Zr in the solid solution decrease approaching equilibrium concentrations. Unfortunately, it is not possible to determine separately the concentrations of these elements in the solid solution at a given solution treatment time *t*. However, by knowing the initial super-saturated concentrations of Sc and Zr in the alloy and the volume fraction of the precipitated $Al_3(Sc,Zr)$ particles at a time *t*, the amounts of Sc+Zr remaining in the supersaturated solid solution after different heat treatment can be estimated using equation (A4) of Appendix 1:

$$C_{Sc+Zr}(f_V) = C_{Sc+Zr}(0) - f_V[Cp(a_1/a_2)^3 - C_{Sc+Zr}(0)] \quad (5)$$

Here $C_{Sc+Zr}(0)$ and $C_{Sc+Zr}(f_V)$ are the concentrations (in mole fractions or in at%) of Sc+Zr in the Al matrix before and after precipitation of the f_V volume fraction of the $Al_3(Sc,Zr)$ particles; a_1 and a_2 are the lattice parameters of Al and $Al_3(Sc,Zr)$ phases, respectively; and Cp (=25%) is the concentration of Sc+Zr in the $Al_3(Sc,Zr)$ phase. Using a_1 = 0.403 nm, a_2 = 0.409 nm, $C_{Sc+Zr}(0)$ = 0.17 at%, and the values of f_V given in Table 2, the concentrations of Sc+Zr in the supersaturated solid solution after different solution treatment were calculated and the results are presented in Figure 9. It can be seen that the sum concentration of these elements in the Al matrix continuously decreases with an increase in the solution treatment time and the concentration is smaller after the treatment at 480ºC than at 460ºC. Nevertheless, even after holding at 480ºC for 48 hours the concentration of Sc+Zr (~0.065 at%) is still above the equilibrium saturated concentration of these elements at 480ºC. Indeed, the equilibrium solubility of these elements in fcc-Al in binary Al-Zr and Al-Sc alloys at 480ºC has been reported to be 0.012 at% Zr [17] and 0.025 at% Sc [18], respectively, which leads to 0.037 at% Sc+Zr. The presence of other alloying elements can further decrease the solvus concentrations of Zr and Sc [19]. For example, using Alcoa thermodynamic database, the maximum solubility of Zr and Sc in the 7050 Al alloy at 480ºC has been estimated to be 0.016 at% [19]. Considering the equilibrium concentration of Sc+Zr at 480ºC as $C_{Sc+Zr}(\infty) \approx 0.037$ at%, the equilibrium volume fraction of the $Al_3(Sc,Zr)$ particles is estimated, using Equation (A5) from Appendix 1, to be $f_V^{\infty} = 5.6\text{x}10^{-3}$. At $C_{Sc+Zr}(\infty) \approx 0.016$ at%, f_V^{∞} is estimated to be $6.5\text{x}10^{-3}$. One can therefore conclude that the $Al_3(Sc,Zr)$ particle growth in the SSA018 alloy during solution treatment at 460ºC and 480ºC occurs under considerable supersaturation.

Particle Size Distribution and the Average Particle Size

The size distributions (PSDs) of the $Al_3(Sc,Zr)$ particles precipitated during solution treatment of the SSA018 alloy were determined after different solution treatment times and temperatures with a rather high statistics (1000 to 16000 particles per the condition, depending on the particle number density). These PSDs were found to be nearly symmetric (see Figure 5) and can be well fitted by the normal distribution (Gaussian) function (Equation 1). There is a strong linear correlation between the reciprocal standard deviation, σ^{-1}, and the pre-exponential term, *C,*

values for all twelve PSDs obtained in this work (Figure 10a), which supports the Gaussian nature of these distributions.

Our attempts to use PSD functions derived from the classical Lifshitz-Slyozov-Wagner (LSW) [20,21], Ardell [22], Brailsford and Wynbladt [23], Voorhees and Glickman [24] and other theories describing the Ostwald ripening process (see [25] for a detailed review) were unsuccessful, because at the particle volume fractions $f_V < 0.01$ (which is our case) all these theories predict highly non-symmetrical PSDs, with a sharp cutoff of the distribution near the particle diameter $d = 1.5\,\bar{d}$, where $\bar{d}$ is the average particle diameter. This discrepancy between the experimental and theoretical PSDs for the particle growth is not unusual, but agrees well with many other observations. In fact, virtually none of the previously reported particle size distributions are of the form predicted by the LSW theory; they are generally broader and more symmetric (for example, see Figure 1 in ref. 25, where PSDs from different alloys are shown). Modified LSW theories can lead to near symmetrical distribution, but only at high volume fractions ($f_V > 0.1$) [25]. The fact that the experimental PSDs are also symmetric at very low volume fractions of precipitates may indicate that not only the particle volume fraction but some other quantity/condition of the system, which has not been taken into account in the Ostwald ripening theories, is responsible for the near-symmetric distribution. Indeed, analysis of these theories shows that they all use a continuity equation for the particle size distribution function, $\Phi(r,t)$, in the form:

$$\frac{\partial \Phi}{\partial t} + \frac{\partial}{\partial r}\left(\omega \Phi\right) = 0 \qquad (6)$$

On the other hand, the distribution function of a stochastic process is generally described by a Fokker-Planck equation [26,27]:

$$\frac{\partial \Phi}{\partial t} + \frac{\partial}{\partial r}\left(\omega \Phi\right) = D^* \frac{\partial^2 \Phi}{\partial r^2} \qquad (7)$$

In Equations (6) and (7) r is the particle radius, $\omega = dr/dt$ is the rate of particle growth and D^* is a diffusion (stochastic) related parameter. The term on the right side of Equation (7) is zero for

non-stochastic processes only. In the case of the particle growth/coarsening, in addition to the concentration-gradient-induced atom flux, atoms can also stochastically enter and exit the particles; the latter process would result in a stochastic force, $\Gamma(t)$. By definition, the average of this force over the system is zero, $<\Gamma(t)> = 0$, while $<\Gamma(t)\Gamma(t')> = D^*\delta(t-t')$, where $\delta(t-t')$ is the delta function [26,27]. Unfortunately, such stochastic process was not taken into account in the cited Ostwald ripening theories and, we believe, this is the main reason of the discrepancy between the theoretical and experimental particle size distributions. At the same time, because $<\Gamma(t)> = 0$, the average values of the particle growth/coarsening process, such as the average particle size and the average growth rate, are not affected by the stochastic process, which explains excellent agreement of the theories with the experiment in describing the evolution of these averaged quantities.

The normal particle size distribution described by Equation (1) can be obtained from Equation (7) if $\omega = d(d_m)/dt$ and $D^* = 0.5d(\sigma^2)/dt$, and both ω and D^* are time dependent. In this case, the term containing ω in Equation (7) describes the drift of the PSD along the r axis and the term containing D^* describes the change of the width of the PSD with time. We can therefore conclude that precipitation and growth of the $Al_3(Sc,Zr)$ particles in the SSA018 alloy studied in this work is a stochastic process.

Figure 10b plots the standard deviation values of the PSDs shown in Figure 5 versus mean diameter of the $Al_3(Sc,Zr)$ particles after twelve different heat treatment conditions. A clear linear dependence of σ on d_m is seen, which can be described by equation

$$\sigma = 1.0 + a_1 d_m \quad \text{(nm)} \qquad (8)$$

where $a_1 = 0.327$. This indicates that there should be a relationship between ω and D^* in our case, i.e. $D^* = (1 + a_1 d_m)a_1\omega$, and the drift and broadening of the PSDs occur synchronously during heat treatment (see Figure 5).

Time Dependence of the Particle Size

The rate of growth of nanometer-sized spherical particles of radius r in a supersaturated solid solution of a concentration c_B follows the equation [28]:

$$\frac{dr}{dt} = \frac{2\gamma V_m c_\infty}{R_g T(1/D + 1/k_d r)}\left(\frac{1}{r r_B(c_B)} - \frac{1}{r^2}\right) \quad (9)$$

In (9), γ is the interfacial energy, V_m is the molar volume of the particle, c_∞ is equilibrium saturated concentration of a solute B in the matrix at an absolute temperature T, R_g is the universal gas constant, D is the diffusion coefficient of the solute, k_d is the rate constant of a first order deposition reaction and $r_B(c_B)$ is a characteristic radius, which depends on c_B through the Gibbs-Thompson equation:

$$c_B = c_\infty \exp\left(\frac{2\gamma V_m}{r_B R_g T}\right) \approx c_\infty\left(1 + \frac{2\gamma V_m}{r_B R_g T}\right) \quad (10)$$

The approximation of the exponential term with the linear terms in Equation (10) was shown to be valid for $r_B > 3\frac{2\gamma V_m}{R_g T}$ [29]. In the case of $Al_3(Sc,Zr)$ particles, for which $\gamma \approx 0.1$ J/m^2 [18,38,39,30] and $V_\mathrm{m} = 1.03\text{x}10^{-5}$ m^3/mol, $\frac{2\gamma V_m}{R_g T} \approx 0.33$ nm at T=753K, i.e. r_B values must be larger than 1 nm. Taking into account that r_B is close to the average particle radius $\bar{r}$ [20,21,29] and, therefore, much above 1 nm (see Table 2), we conclude that the linear approximation of equation (10) is valid to describe our data.

If $D << k_\mathrm{d} r$, the particle growth rate is controlled by diffusion and Equation (11) reduces to

$$\frac{dr}{dt} = \frac{2\gamma V_m c_\infty D}{R_g T r^2}\left(\frac{r}{r_B(c_B)} - 1\right) \quad (11)$$

It is postulated in the LSW theory that the ratio r/r_B does not change with time and $r_B = \bar{r}$. This gives the dependence of the average particle radius, $\bar{r}$, on time

$$\bar{r}^3 - \bar{r}_0^3 = K_1 t \quad (12)$$

where $\bar{r}_0$ is the average radius of the particles at t = 0, and K_1 is a rate constant, which value depends on the particle volume fraction and the shape of the particle size distribution [25]. The LSW theory gives $K_1 = \frac{8\gamma V_m c_\infty D}{9R_g T}$ [20]. If $D >> k_d r$ in Equation (11), then the particle growth rate is controlled by the surface reaction, and the dependence of the average particle size on time is given by

$$\bar{r}^2 - \bar{r}_0^2 = K_2 t \qquad (13)$$

where $K_2 = \frac{2\gamma V_m c_\infty k_d}{R_g T}$ [21].

To recognize the mechanism responsible for the $Al_3(Sc,Zr)$ particle growth and coarsening in the SSA108 alloy, the dependences of the mean particle size on the solution treatment time (see Table 2 and Figure 6) were re-plotted in coordinates $(d_m)^n$ vs. t, at n = 3 (Figure 11) and n = 2 (Figure 12) and fitted with Equations (12) and (13). The fitting parameters, as well as the coefficient of determination R^2 of the respective fits are given in Table 5. Figures 11 and 12 illustrate that both equations fit the experimental data very well, thus making the selection of the controlling mechanism quite difficult. It is likely that the rate of the volume diffusion of Sc/Zr and the rate of reaction at the particle/matrix interfaces are similar, and the particle growth is controlled by a combination of these two mechanisms [28,31]. It is worth to note that the rate constants, K_1 and K_2, depend on the heating rate to the solution treatment temperature, providing faster growth of the particles in the material heated with a slower heating rate. The only parameters responsible for such behavior are γ, D and k_d and a higher value of at least one of them is required to explain the faster particle growth in the slower heated alloy.

The temperature dependences of the diffusion coefficients of Sc and Zr in Al are given by [32,33,34]:

D_{Sc} (cm^2/s) = 5.31 exp(-173 kJ/mol/R_gT)

D_{Zr} (cm^2/s) = 728 exp(-242 kJ/mol/R_gT)

Because Sc diffuses much faster than Zr, in the slower heated alloy (as compared to the faster heated one) more Sc would be present in the particles and less in the solution when the solution treatment temperature is approached, which should lead to a slower apparent diffusion of (Sc+Zr) and slower particle coarsening during isothermal holding. Thus this scenario provides just opposite effect to the experimental observation, which may indicate that the growth rate is not a diffusion controlled process in this case.

The matrix/particle interface energy γ can increase with an increase in the particle size due to transition of the interfaces from a coherent state to a semi-coherent state. However, our TEM studies revealed that the $Al_3(Sc,Zr)$ particles remained fully coherent in the studied particle size range. This observation is supported by recent work of Iwamura and Miura [35] who reported coherent-to-semicoherent transition of the $Al_3(Sc)$ particles in a binary Al-0.2wt% Sc alloy in the particle size (diameter) range of 30 to 80 nm. Moreover, accelerated particle growth was observed only at the particle sizes above 80 nm, while delay in the particle coarsening was noticed in the particle size range of 30-80 nm where coherent and semi-coherent particles coexisted. A small (~5%) increase in γ with an increase in d due to a capillary effect was predicted by a cluster dynamic model [14], while segregation of Zr at the matrix/particle interfaces was reported [36] to decrease in the lattice mismatch and thus decrease in the elastic stress, which is required to maintain coherency.

Although no data on the k_d values for Zr and Sc deposition reaction at the $Al/Al_3(Sc,Zr)$ interfaces is yet available, one may suggest that the deposition rate for Zr is higher. Indeed, addition of Zr to an Al_3Sc particle is more thermodynamically favorable than addition of Sc, as the former leads to a decrease in the elastic energy due to a decrease in the lattice mismatch between the particle and the matrix. Assuming that D and γ values are almost the same in slower and faster heating specimens, k_d = 41 nm/s and 29 nm/s are estimated for Zr and Sc, respectively, at 480ºC.

Kinetics of the Isothermal Phase Transformation

The kinetics of the isothermal phase transformation can generally be described by the Kolmogorov-Johnson-Mehl-Avrami (KJMA) relationship:

$$X(t) \equiv f_V(t)/f_V(\infty) = 1 - \exp(-K_3 t^m) \quad (14)$$

where K_3 and m are the Avrami rate constant and the Avrami exponent, respectively. For the diffusion-controlled growth of spherical particles from pre-existing nuclei, the KJMA theory predicts $m = 1.5$ [37]. To check whether Equation (14) applies to the particle growth process, the experimental data were plotted in coordinates ln(-ln(1-X)) versus ln(t) and fitted with Equation (14) (Figure 10). Very good linear fits were found in these coordinates at $m = 0.404$ and the K_3 values of 1.20×10^{-2} s^{-m}, 1.31×10^{-2} s^{-n}, and 7.45×10^{-3} s^{-m}, for the heat treatments 20-480, 60-480, and 60-460, respectively, indicating that the KJMA relationship may apply for this process. Using the identified parameters m and K_3, the time dependences of the precipitate volume fraction were calculated for different heat treatment conditions and plotted as dashed lines in Figure 14, together with the experimental data points. It can be seen that the calculated dependences give typical sigmoidal curves for f_v vs. ln(t) and indicate that, in the semi-logarithmic coordinates, the particle growth process after 48 hours at 460°C is on the second, accelerating stage, while after 48 hours at 480°C, it already approaches the third stage, at which the reaction slows down approaching equilibrium. Accordingly, a decrease in the concentration of Sc+Zr in the Al matrix with an increase in the solution treatment time also follows the sigmoidal behavior (see the dashed curves in Figure 9, which were calculated using Equations 14 and 5).

The low value of $m = 0.404$ obtained for the process of precipitation of the $Al_3(Sc,Zr)$ particles definitely indicates that no nucleation was involved during isothermal holding at 460°C or 480°C, i.e. all the particles were already formed during the preceding stage of heating to the temperature [37]. This result agrees well with previous results on precipitation of the Al_3Sc, Al_3Zr and $Al_3(Sc,Zr)$ particles in binary and ternary Al-Sc-Zr alloys [14,15,16,38,39]. However, this value of $m = 0.404$ is much smaller than the value of 1.5, which the theory predicts for the three-dimensional diffusion controlled growth process [37]. Similar small values of m have already been observed during precipitation of spherical particles of the second phase in some other systems [40,41,42], including Al-Sc alloys at high temperatures and/or late stages of precipitation [38,43]; therefore, this result of our work is not unique. Unfortunately, there is still not clear theoretical explanation, what growing mechanism provides such a small value of m in the KJMA during the three-dimensional particle growth. A mechanism of the particle growth

controlled by a reaction at the matrix/particle interface, which provided the value of m = 1/3, was proposed [41]. In that mechanism, the particle growth was controlled by diffusion of a solute from the matrix into the particle along an array of misfit dislocations located at the matrix/particle semi-coherent interfaces. It is likely that the small value of m obtained in our work indicates that the growth of the $Al_3(Sc,Zr)$ particles is controlled by the reaction at the matrix/particle interface, although the specific mechanism of this reaction is not identified.

EFFECT OF $Al_3(Sc,Zr)$ PARTICLES ON TENSILE PROPERTIES

A room temperature strength increase due to precipitation of the $Al_3(Sc,Zr)$ particles can generally occur by means of two mechanisms, depending on the particle size. These are (i) shearing mechanism of small precipitates, which involves order strengthening, coherency strengthening, and modulus mismatch strengthening; and (ii) the Orowan bypass mechanism for larger particles, when dislocations cannot move through but looping around the particles [44]. With an increase in the particle diameter, the yield strength increases when the first mechanism operates, while it decreases when the Orowan mechanism operates. According to recent studies of binary Al-Sc alloys, transition from the shearing mechanism to Orowan strengthening mechanism occurs in the particle diameter range between 4 to 6 nm [45,46], suggesting that the Orowan mechanism should be responsible for the $Al_3(Sc,Zr)$ particle induced strengthening in our case. An observed decrease in the yield strength with an increase in the particle diameter (see Figure 8) supports this suggestion.

The increase in the yield stress due to the Orowan strengthening, $\Delta\sigma_{Or}$, is given by [47,48]:

$$\Delta\sigma_{Or} = K_4 M(1-\nu)^{-0.5}(Gb/\lambda)\ln(d_s/b) \qquad (15)$$

where M is the Taylor factor, ν and G are the matrix Poisson's ratio and the shear modulus, respectively, b is the magnitude of the Al matrix Burgers vector, K_4 is a constant, which value depends on the particle size distribution, and d_s and λ are the mean particle diameter and an effective inter-particle distance, respectively, both on the dislocation slip planes. For mono-

dispersed assembly of the precipitates, $K_4 \approx 0.127$, $d_s = \pi d_m/4$, and $\lambda = \left[\frac{1}{2}\left(\frac{2\pi}{3f_V}\right)^{0.5} - 1\right]\frac{\pi d_m}{4}$ [44,47].

Figures 15a and 15b show the dependences of the yield strength of the SSA018 alloy in W24 temper (solution treatment, water quenching and holding at room temperature for 24 hours) on $\lambda^{-1}\ln(\pi d_m/4b)$ and d_m, respectively. The calculated Orowan strength values are also shown there as open symbols (for the experimentally determined diameters and volume fractions of the $Al_3(Sc,Zr)$ particles given in Table 2 for different specimens) and as a solid line [for a continuously increasing variable of $\lambda^{-1}\ln(\pi d_m/4b)$, Equation 15]. The following values of the parameters of Equation 15 were used to calculate $\Delta\sigma_{Or}$: $K_4 = 0.127$, $M = 3.06$ (a non-textured alloy), $\nu = 0.331$ and $G = 27.8$ GPa [49], and $b = 0.286$ nm, so that the Orowan strength in the SSA018 alloy related to the $Al_3(Sc,Zr)$ particles can be expressed as:

$$\Delta\sigma_{Or} = 13209(b/\lambda)\ln(\pi d_m/4b) \text{ (MPa)} \qquad (16)$$

Figure 15 illustrates that the $Al_3(Sc,Zr)$ particles formed in the DC cast SSA018 alloy during solution treatment provide additional Orowan strengthening, which decreases from ~118 MPa to ~75 MPa with an increase in the particle diameter from 10.4 nm to 27.3 nm. It is interesting to note that the maximum value of $\Delta\sigma_{Or}$ is achieved at the particle diameter of 10.4 nm, and $\Delta\sigma_{Or}$ does not change or even slightly decreases with a further decrease in the particle diameter, which is due to a considerably reduced volume fraction of the smaller particles (see Table 2) and a noticeable effect of the logarithmic term (Equation 16) at decreasing d_m values. For example, after solution treatment at 460°C, the Orowan stress (open triangles in Figure 15b) almost does not depend on the $Al_3(Sc,Zr)$ particle size and is about 105 MPa.

The experimental values of YS of all specimens, except two ones, follow a linear dependence on the $\lambda^{-1}\ln(\pi d_m/4b)$ variable, with almost the same slop as the Orowan strength dependence has (see Figure 15a). When $\Delta\sigma_{Or}$ is subtracted from the YS, a resulting stress of $\Delta\sigma_{W24} = 187$ MPa is obtained, which correspond to the yield stress of the alloy without the $Al_3(Sc,Zr)$ particles in W24 temper. One can see that the contribution from these particles to the yield stress in W24

temper is rather noticeable and makes up from 40% to 63%. The YS values of two specimens, which were solution treated at 460°C for 1 hour and 4 hours, do not follow the linear (Orowan) dependence on $\lambda^{-1}\ln(\pi d_m/4b)$ and they are ~10-30 MPa higher than those expected from the Orowan mechanism. The reason of such "anomalous" behavior was not identified in this work. We may however suggest that this additional strengthening (~10-30 MPa) can be due to incomplete dissolution of the eutectic phases, which were present in the DC cast alloy.

A substantial increase in the room temperature strength after artificial aging at 120°C is evidently related to the precipitation of the *GP II* zones and η' particles during aging [12,13]. The strengthening effect from *GP II* and η' is much stronger than that from the $Al_3(Sc,Zr)$ particles. Figure 16 shows dependence of the YS of the SSA018 alloy after different solution treatment conditions and aging at 120°C for 19 hours on the Orowan strengthening term $\lambda^{-1}\ln(\pi d_m/4b)$. The dashed line in the figure is described by relation:

$$YS = \Delta\sigma_{Or} + 417 \text{ (MPa)} \qquad (17)$$

where $\Delta\sigma_{Or}$ is given by Equation (16). This analysis indicates that the DC cast SSA018 alloy without fine $Al_3(Sc,Zr)$ particles should have the average yield stress of $\Delta\sigma_{T6} = 417$ MPa after T6 temper. Thus the contribution to the total YS of the alloy after T6 temper from the $Al_3(Sc,Zr)$ particles is only 18% to 28% of $\Delta\sigma_{T6}$. Taking into account that the yield stress of the alloy without the $Al_3(Sc,Zr)$ particles and before artificial aging is $\Delta\sigma_{W24} = 187$ MPa, the average stress increase due to the artificial aging, $\Delta\sigma_{AA}$, is estimated to be $\Delta\sigma_{AA} = 230$ MPa.

It should be noted that both a higher solution treatment temperature and longer solution treatment time result in more complete dissolution of Zn-, Mg-, and Cu-rich phases, which should lead to a higher number density of the *GP II* zones and η' particles and, therefore, a higher value of $\Delta\sigma_{T6}$ after artificial aging. On the other hand, the higher solution treatment temperatures and longer times result in coarser $Al_3(Sc,Zr)$ particles and, therefore, a decreasing value of $\Delta\sigma_{Or}$. Therefore, the solution treatment conditions of the Sc (and Zr) containing alloy should be optimized in order to achieve the highest values of $YS = \Delta\sigma_{Or} + \Delta\sigma_{T6}$. Pre-solution treatment seems to be important for precipitation of higher number density and finer $Al_3(Sc,Zr)$ particles. The lower temperature precipitation should also lead to core-shell nanoparticles, where the core is enriched with Sc and

the shell is enriched with slower-diffusing Zr atoms [16]. Such a core-shell structure is believed to slow down coarsening process during following solution treatment [50] and may benefit in a further increase in the tensile strength.

CONCLUSIONS

The effect of solution heat treatment regimes on the microstructure and tensile properties of a direct chill cast Al-Zn-Mg-Cu-Sc-Zr SSA018 alloy was studied. The following results were obtained.

1. During solution treatment, precipitation and growth of fine coherent $Al_3(Sc,Zr)$ particles from a super-saturated solid solution occurred. An increase in the solution treatment temperature from 460^{o}C to 480°C resulted in the $Al_3(Sc,Zr)$ particles with a larger mean diameter, higher volume fraction and lower number density. At both temperatures the precipitation reaction occurred rather slow and even after holding for 48 hours the reaction was complete by ~ 65% at 460^{o}C and ~ 75-80% at 480^{o}C.
2. The distributions of the particles by sizes were symmetrical after all studied solution treatment conditions and were well described by a normal (Gaussian) distribution function, but they did not follow the LSW theories of Ostwald ripening. The main reason of disagreement between the theoretical and experimental particle size distributions (PSDs) was found to be in ignoring stochastic processes during particle growth and coarsening. Taking into account the stochastic process led to an additional (stochastic-process-related) term in a continuity equation, which thus transformed to a Fokker-Planck equation. Under certain boundary conditions this equation describes well the experimental PSDs, indicating stochastic nature of the precipitation and growth process of the $Al_3(Sc,Zr)$ particles. The standard deviation, σ, and the mean particle size, d_m, of the PSDs were linear dependent, so that an increase in d_m led to PSD broadening.
3. The time dependence of the mean particle size was well described by both the diffusion-controlled and interface-reaction controlled processes. Analysis of the effect of heating rate on growth and analysis of the transformation kinetics led to selection of the reaction-limited process as a likely growth controlling process. It is also possible that the particle growth was controlled by a combination of both processes.

4. The kinetics of the isothermal phase transformation (precipitation and growth at a continuously increasing volume fraction of the $Al_3(Sc,Zr)$ particles) was well described by the Kolmogorov-Johnson-Mehl-Avrami (KJMA) law, with the Avrami exponent $m = 0.404$. The small value of m may indicate that the growth of the $Al_3(Sc,Zr)$ particles is controlled by the reaction at the matrix/particle interface, although the specific mechanism of this reaction was not identified.
5. The coherent nanometer-sized $Al_3(Sc,Zr)$ particles formed during solution treatment provided an additional Orowan strengthening of the SSA018 alloy, which increased with a decrease in the particle size and an increase in the particle volume fraction and varied from 75 MPa to 118 MPa after different heat treatment used in this work. After solution treatment and holding at room temperature for 24 hours, the Orowan strengthening from these particles provided from 40% to 63% of the yield strength increase relative to the alloy without the nanometer-sized $Al_3(Sc,Zr)$ particles. After aging at 120°C for 19 hours, the substantial increase in both the yield strength and the ultimate strength was observed that was related to the precipitation of the *GP II* zones and η' phase particles while the $Al_3(Sc,Zr)$ particles provided ~ 18% to 28% of the yield strength increase of the alloy without these particles, which corresponded to ~ 15% to 22% of the total yield strength.

ACKNOWLEDGEMENTS

The authors thank Dr. R. Wheeler, UES Inc. (Dayton, OH), for useful technical discussions. This work was financially supported through the United States Air Force Contracts No. F04611-02-C-0014 (Capt. William Allen, Program Manager) and No. FA8650-04-D-5233 (Dr. J. Fuller, Program Manager).

APPENDIX 1. THE CONCENTRATION OF A SOLUTE IN A SUPERSATURATED SOLID SOLUTION DURING PRECIPITATION

Let consider a matrix with the crystal unit cell volume of Ω_1 and the number of the lattice sites per unit cell of n_1. An alloying element B is present in the matrix in a supersaturated solid solution with an initial concentration of $C_1^B(0)$ (the concentration is in atomic %). Because of

the supersaturation, the solute *B* precipitates into a second phase, which has the unit cell volume of Ω_2, the number of the lattice sites per unit cell of n_2 and the concentration of the element *B* of C_2^B. We assume that C_2^B does not change during precipitation. Due to formation of the second phase in the amount of f_V, the concentration of the element B in the matrix decreases to $C_1^B(f_V)$, which dependence on f_V is determined below.

Before precipitation, the number of the *B* atoms per unit volume in the matrix is

$$N_1^B(0) = \frac{C_1^B(0)}{100}\frac{n_1}{\Omega_1} \qquad \text{(A1)}$$

After the second phase is formed in the amount of f_V, the element *B* is distributed between the matrix and the second phase. The number of the *B* atoms in the second phase, per unit volume, is

$$N_2^B(f_V) = \frac{C_2^B}{100}\frac{f_V n_2}{\Omega_2}, \qquad \text{(A2)}$$

while their number in the matrix is

$$N_1^B(f_V) = \frac{C_1^B(f_V)}{100}\frac{(1-f_V)n_1}{\Omega_1} = N_1^B(0) - N_2^B(f_V) \qquad \text{(A3)}$$

Combining (A1), (A2), and (A3) and assuming that $f_V \ll 1$, the dependence of C_1^B on the volume fraction of the second phase, f_V, is obtained:

$$C_1^B(f_V) = C_1^B(0) - f_V\left[C_2^B\frac{n_2\Omega_1}{n_1\Omega_2} - C_1^B(0)\right] \qquad \text{(A4)}$$

The maximum volume fraction of the second phase, which can precipitate in the matrix, is then determined as:

$$f_V(\infty) = \frac{C_1^B(0) - C_1^B(\infty)}{C_2^B\frac{n_2\Omega_1}{n_1\Omega_2} - C_1^B(0)} \qquad \text{(A5)}$$

where $C_1^B(\infty)$ is the equilibrium concentration of element B in the matrix phase.

REFERENCES

1 J.G. Kaufman (Ed.), Properties of Aluminum Alloys: Tensile, Creep, and Fatigue Data at High and Low Temperatures, ASM International, Materials Park, OH, 1999.

2 J.R. Davis (Ed.), Aluminum and Aluminum Alloys, ASM Specialty Handbook, ASM International, Materials Park, OH, 1993.

3 V.I. Elagin, Technology of Light Alloys (Tekhnologiya Legkikh Splavov, USSR), No. 9 (1994) 5-14.

4 V.I. Elagin, V.V. Zakharova, T.D. Rostova, Met.Sci. Heat Treatment, 36 (7-8) (1995), 375-380.

5 O.N. Senkov, R.B. Bhat, S.V. Senkova, In: Metallic Materials with High Structural Efficiency, O.N. Senkov, D.B. Miracle, S.A. Firstov, eds., Kluwer Academic Publishers, Dordrecht, The Netherlands, 2004, pp. 151-162.

6 Y.V. Milman, A.I. Sirko, D.V. Lotsko, D.B. Miracle, O.N. Senkov, Mater. Sci. Forum, 396-402 (2002) 1217-1222.

7 A.F. Norman, K. Hyde, F. Costello, S. Thompson, S. Birley, P.B. Pragnell, Mater. Sci. Eng. A, 354 (2003) 188-198.

8 O.N. Senkov, R.B. Bhat, S.V. Senkova, J.D. Schloz, Metall. Mater. Trans. A, 36A (2005) 2115-2126.

9 Y.W. Riddle, T.H. Sanders Jr., Mater. Sci. Forum, 331-337 (2000) 939-944.

10 J. Royset, N. Ryum, Internat. Mater. Rev., 50 (2005) 19-44.

11 O.N. Senkov, S.V. Senkova, M.G. Mendiratta, D.B. Miracle, U.S. Patent No. 7048815, May 23, 2006.

12 M.R. Shaghiev, O.N. Senkov, and S.V. Senkova, in: *Materials Science &Technology (MS&T) 2006: Materials and Systems, Vol. 2*, (The Minerals, Materials and Metallurgical Society, Warrendalle, PA, 2006) pp. 213-222.

13 O.N. Senkov, M.R. Shaghiev, S.V. Senkova, Metall. Mater. Trans. A (submitted in 2007).

14 E. Clouet, A. Barbu, L. Lae, G. Martin, Acta Mater. 53 (2005) 2313-2325.

15 H. Hallem, W. Lefebvre, B. Forbord, F. Danoix, K. Marthinsen, Mater. Sci. Eng. A 421 (2006) 154-160.

16 E. Clouet, L. Lae, T. Epicier, W. Lefebvre, M. Nastar, A. Deschamps, Nature Materials, 5 (2006) 482-488.

17 J. Murray, A. Peruzzi, and J.P Abriata, J. Phase Equilibria, 13 (1992) 277-291.

18 H.H. Jo and S.I. Fujikawa, Mater. Sci. Eng. A171 (1993) 151-161.

19 J.D. Robson, Acta Materialia, 52 (2004) 1409-1421.

20 I.M. Lifshitz and V.V. Slyozov, J. Phys. Chem. Solids, 19 (1/2) (1961) 35-50.

21 C. Wagner, Z. Electrochem. 65 (1961) 581-591.

22 A.J. Ardell, Acta Metallurgica, 20 (1972) 61-71.

23 A.D. Brailsford and P. Wynblatt, Acta Metallurgica, 27 (1979) 489-497.

24 P.W. Voorhees and M.E. Glicksman, Acta metallurgica 32 (1984) 2001-2030.

25 A. Baldan, J. Mater. Science 37 (2002) 2171-2202.

26 H. Risken, The Fokker-Plank equation. Methods of Solution and Applications, Springer-Verlag, Berlin, 1984.

27 C.W. Gardiner, Handbook of Stochastic Methods for Physics, Chemistry and the Natural Sciences, Third Edition, Springer, Berlin, 2004.

28 R. Viswanatha and D.D. Sarma, in: C.N.R. Rao, A. Muller, and A.K. Cheetham (Eds.) Nanomaterials Chemistry, Wiley-VCH, Weinheim, 2007, pp. 139-170.

29 R. Wagner and R. Kampmann, in: R.W. Cahn, P. Haasen, E.J. Kramer (Eds.) Materials Science and Technology, A Comprehensive Treatment, Vol. 5: Phase transformations in Materials, VCH Publishers, NY, 1991, pp.213-303.

30 K.E. Knipling, D.C. Dunand, and D.N. Seidman, Metal. Mater. Trans. A (2007).

31 D.V. Talapin, A.L. Rogach, M. Haase, H. Weller, J. Phys. Chem. B, 105 (2001) 12278-12285.

32 S. Fujikawa, J. Jpn. Inst. Light Met. 46 (4) (1996) 202-215.

33 S.I. Fujikawa, Defect & Diffusion Forum, 143-147 (1997) 115-120.

34 T. Marumo, S. Fujikawa, K.-I. Hirano, J. Jpn. Inst. Light met. 23 (1) (1973) 17-25.

35 S. Iwamura and Y. Miura, Acta Materialia 51 (2004) 591-600.

36 E. Harada and D.C. Dunand, Mater. Sci. Eng. A 329-331 (2002) 686-695.

37 J.W. Christian, The Theory of Transformation in Metals and Alloys, 2nd Edition, Part 1, Pergamon Press, Oxford, 1975.

38 J. Royset and N. Ryum, Mater. Sci. Eng. A 396 (2005) 409-422.

39 G.M. Novotny, A.J. Ardell, Mater. Sci. Eng. A 318 (2001) 144-154.

40 C.S. Roberts, L. Averbach, and M. Cohen, Trans. Amer. Soc. Metals 45 (1953) 576-.

41 B.S. Lement and M. Cohen, Acta Metall. 4 (1956) 469-.

42 A. Cserei, J. Jiang, F. Aubertin, and U. Gonser, J. Mater. Sci. 29 (1994) 1213-1216.

43 A.L. Berezina, V.A. Volkov, B.P. Domashnikov, S.V. Ivanov, K.V. Chuistov, Phys Met. 10 (1990) 296-304.

44 E. Nembach, Particle Strengthening of Metals and Alloys, John Wiley, NY, 1997.

45 D.N. Seidman, E.A. Marquis, D.C. Dunand, Acta Materialia 50 (2002) 4021-4035.

46 B.A. Parker, mater. Scie. Forum 189 (1995) 347-

47 M.F. Ashby, Strengthening Methods in Crystals, Elsevier, NY, 1971, p.165.

48 L.M. Brown and R.K. Ham, in: A. Kelly and E.B. Nicholson (Eds.) Strengthening Methods in Crystals, Elsevier, Amsterdam, 1971, pp. 9-135.

49 O.N. Senkov, Advanced Aluminum Material for Rocket Turbopump Rotors, SBIR Phase II Special Report, AFRL-PR-ED-TR-2006-0074, Air Force Research Laboratory, Edwards Air Force Base, CA, December, 2006.

50 P.W. Voorhees, Nature Materials 5 (2006) 435-436.

Precipitation of $Al_3(Sc,Zr)$ Particles in a Direct Chill cast Al-Zn-Mg-Cu-Sc-Zr Alloy During Conventional Solution Heat Treatment

Tables

Table 1. Chemical composition (in wt.%) of SSA018 alloy

Element	**Zn**	**Mg**	**Cu**	**Mn**	**Fe**	**Si**	**Zr**	**Sc**	**Al**
Concentration, wt.%	7.17	2.20	1.58	0.3	0.13	0.09	0.18	0.18	Balance
Concentration, at.%	3.13	2.58	0.71	0.156	0.066	0.091	0.056	0.114	Balance

Table 2. Mean size (diameter), d_m, volume fraction, f_V, number density, N, and surface area fraction, f_A, of the secondary $Al_3(Sc,Zr)$ particles in the SSA018 alloy after different heat treatment conditions. The values of the standard deviation of the particle size distribution, σ, and the normalizing parameter, C, from Equation (1) are also given here.

Treatment ID	ST Condition			Microstructural Features of $Al_3(Sc,Zr)$ Particles					
	V (ºC/h)	T (ºC)	t (h)	d_m (nm)	f_V (10^{-4})	N (10^{14} cm^{-3})	f_A (10^3 cm^{-1})	σ (nm)	C (%)
20-480-1	20	480	1	7.9	16	43	9.8	3.55	33.0
20-480-4			4	12.3	26	19	10.4	4.82	25.1
20-480-20			20	18.1	38	7.6	9.5	6.94	16.9
20-480-48			48	27.3	42	3.1	7.1	10.9	11.0
60-480-1	60	480	1	7.4	17	44	9.3	3.96	31.8
60-480-4			4	10.4	26	33	12.6	4.25	28.5
60-480-20			20	17.9	39	10	11.5	6.50	18.4
60-480-48			48	25.2	46	4.2	9.2	8.68	13.8
60-460-1		460	1	6.0	11	54	7.5	2.75	44.2
60-460-4			8	8.6	16	39	7.9	4.44	28.3
60-460-20			20	12.3	26	21	11.2	4.93	24.7
60-460-48			48	16.0	36	13	11.3	5.79	20.8

Table 3. Parameters of Equation (2) for different heat treatment conditions. R^2 is the coefficient of determination of the Equation (2) fit.

Treatment ID	A (nm/s^B)	B	R^2
20-480	0.642	0.31	0.986
60-480	0.531	0.32	0.991
60-460	0.798	0.25	0.998

Table 4. RT tensile properties of the SSA018 alloy after different heat treatments

Solution Treatment ID	W24 temper (Aging at RT for 24 h)			T6 temper (Aging at 120ºC for 19 h)		
	YS MPa	UTS MPa	El %	YS MPa	UTS MPa	El %
20-480-1	-	-	-	536	611	10.5
20-480-4	292	479	16.3	527	608	11.3
20-480-20	279	478	19.8	514	600	12.5
20-480-48	267	465	23.0	499	589	12.3
60-480-1	303	471	15	528	597	8.2
60-480-4	301	480	15	532	613	8.6
60-480-20	280	480	20.3	508	591	11.3
60-480-48	275	477	21.3	495	587	15.0
60-460-1	331	503	15.0	532	592	11.8
60-460-4	309	488	17.0	540	600	8.7
60-460-20	296	485	17.5	519	596	9.2
60-460-48	294	489	16.8	500	582	11.4

Table 5. Parameters of Equations (12) and (13) for different heat treatment conditions. R^2 is the coefficient of determination of the respective fits.

Treatment ID	*Parameters of Equation (12)*			*Parameters of Equation (13)*		
	d_{mo} (nm)	K_1 (10^{-2} nm^3/s)	R^2	d_{mo} (nm)	K_2 (10^{-3} nm^2/s)	R^2
20-480	5.1	11.7	0.985	7.1	4.01	0.994
60-480	4.8	8.99	0.994	6.6	3.49	0.995
60-460	5.3	2.31	0.997	6.2	1.31	0.975

Precipitation of $Al_3(Sc,Zr)$ Particles in a Direct Chill cast Al-Zn-Mg-Cu-Sc-Zr Alloy During Conventional Solution Heat Treatment

FIGURES

(a) 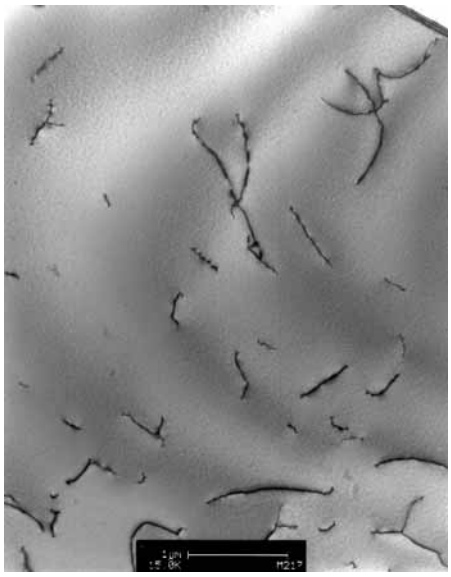 (b) 

Figure 1. TEM images of the Sc-containing alloy in as-cast condition. (a) Individual dislocations inside a grain; (b) an eutectic region. The marker lengths on the figures are (a) 1μm and (b) 0.5 μm.

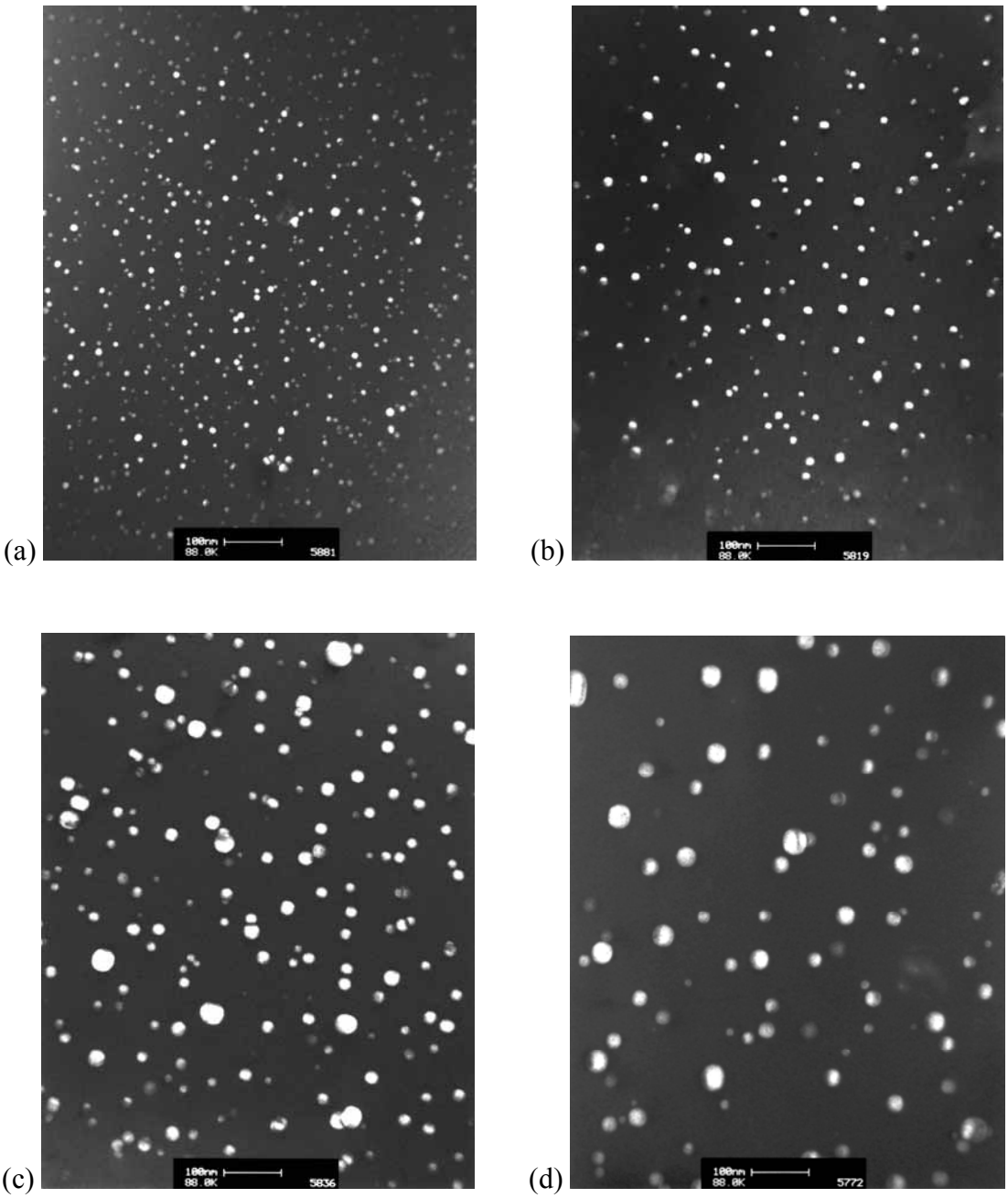

Figure 2. Dark field TEM images in $Al_3(Sc,Zr)$ reflexes of SSA018 alloy after solution treatment (heating from RT to 480ºC with a heating rate of 20ºC/h and holding at 480ºC for different time periods), water quenching and aging at 120ºC for 19 hours. Soaking time at 480ºC was (a) 1 hour, (b) 4 hours, (c) 20 hours, and (d) 48 hours. All images were taken in $\langle 110 \rangle_{Al}$ projection. Corresponding selected area diffraction patterns are given as the inserts. The markers on the figures are 100 nm long.

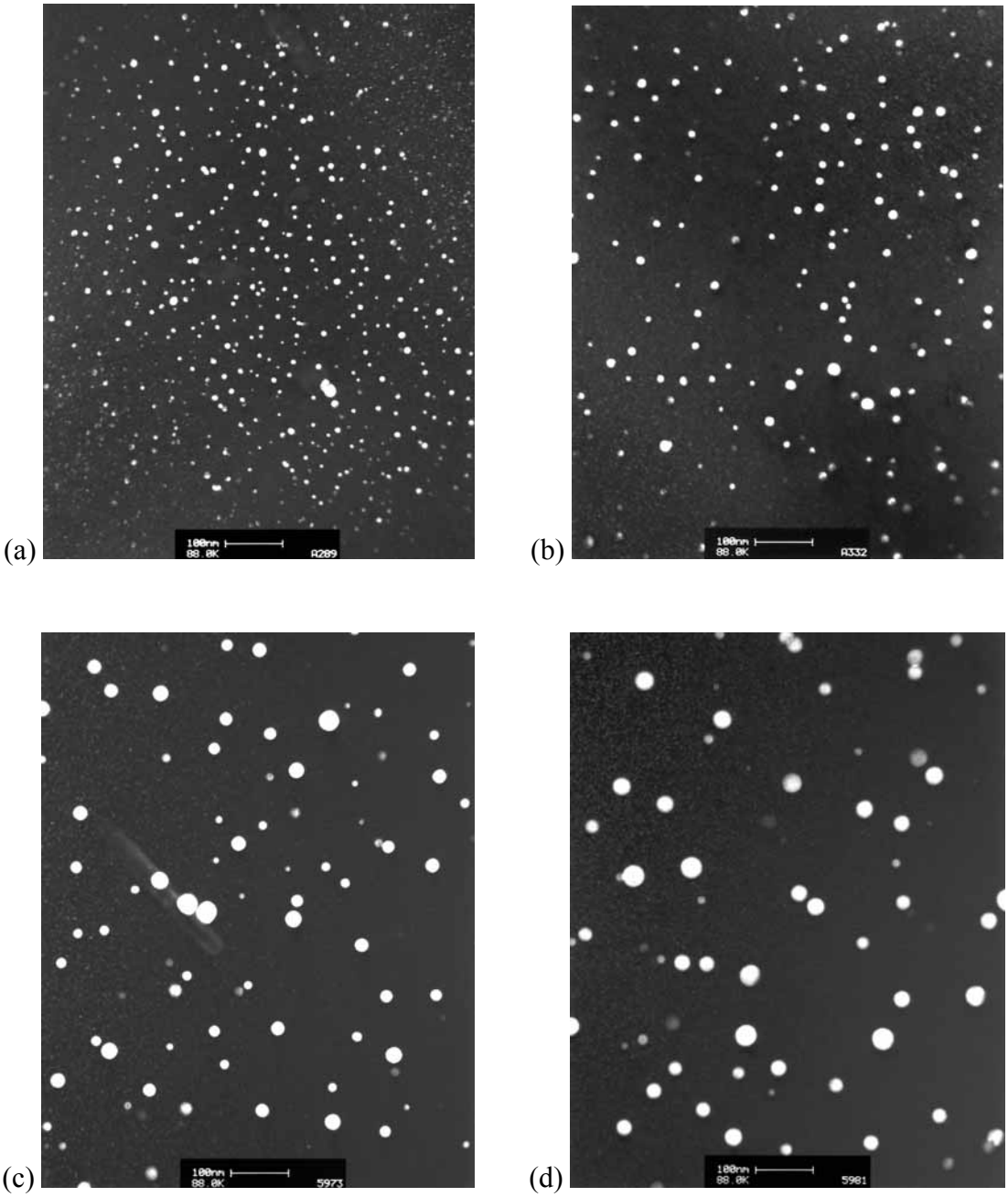

Figure 3. Dark field TEM images in $Al_3(Sc,Zr)$ reflexes of SSA018 alloy after solution treatment (heating from RT to 480ºC with a heating rate of 60ºC/h and holding at 480ºC for different time periods), water quenching and aging at 120ºC for 19 hours. Soaking time at 480ºC was (a) 1 hour, (b) 4 hours, (c) 20 hours, and (d) 48 hours. All images were taken in $\langle 112 \rangle_{Al}$ projection. The markers on the figures are 100 nm long.

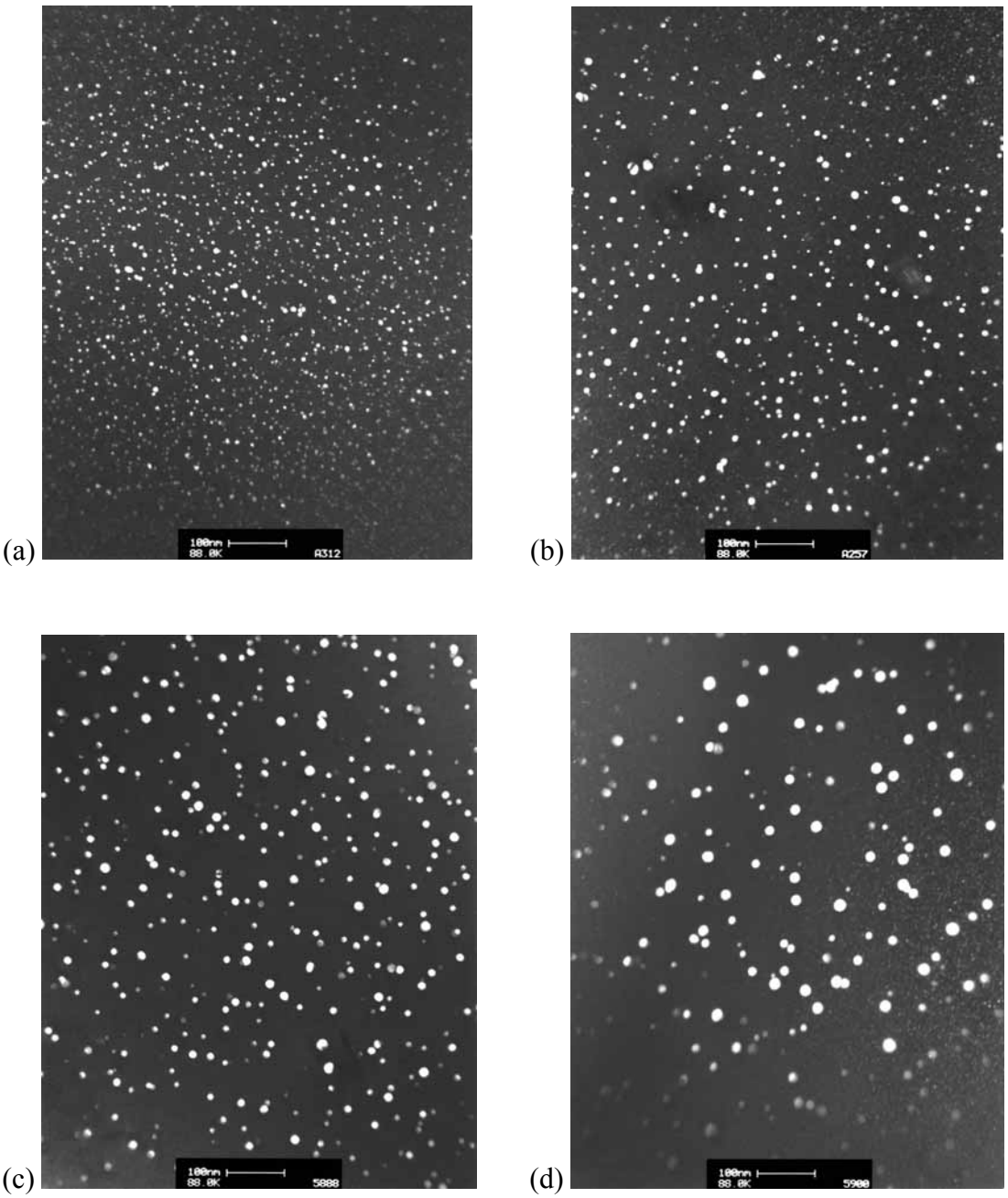

Figure 4. Dark field TEM images in $Al_3(Sc,Zr)$ reflexes of SSA018 alloy after solution treatment (heating from RT to 460ºC with a heating rate of 60ºC/h and holding at 460ºC for different time periods), water quenching and aging at 120ºC for 19 hours. Soaking time at 460ºC was (a) 1 hour, (b) 4 hours, (c) 20 hours, and (d) 48 hours. Images (a) and (b) were taken in $\langle 112 \rangle_{Al}$ projection while (c) and (d) were taken in $\langle 110 \rangle_{Al}$ projection. The markers on the figures are 100 nm long.

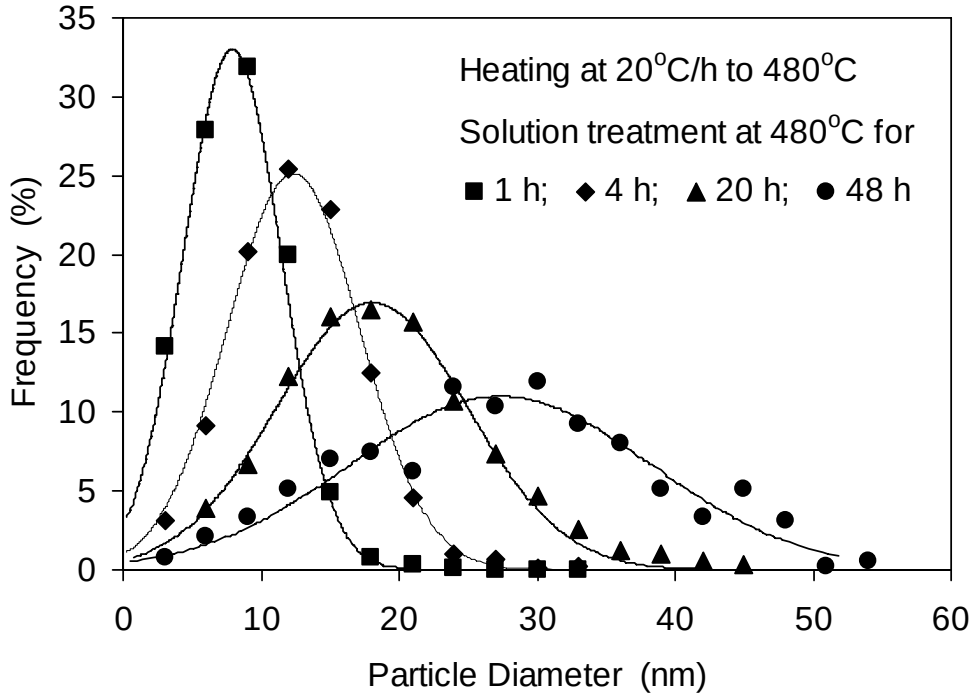
Heating at 20°C/h to 480°C
Solution treatment at 480°C for
1 h; 4 h; 20 h; 48 h
Frequency (%)
Particle Diameter (nm)
0
5
10
15
20
25
30
35
0
10
20
30
40
50
60

(a)

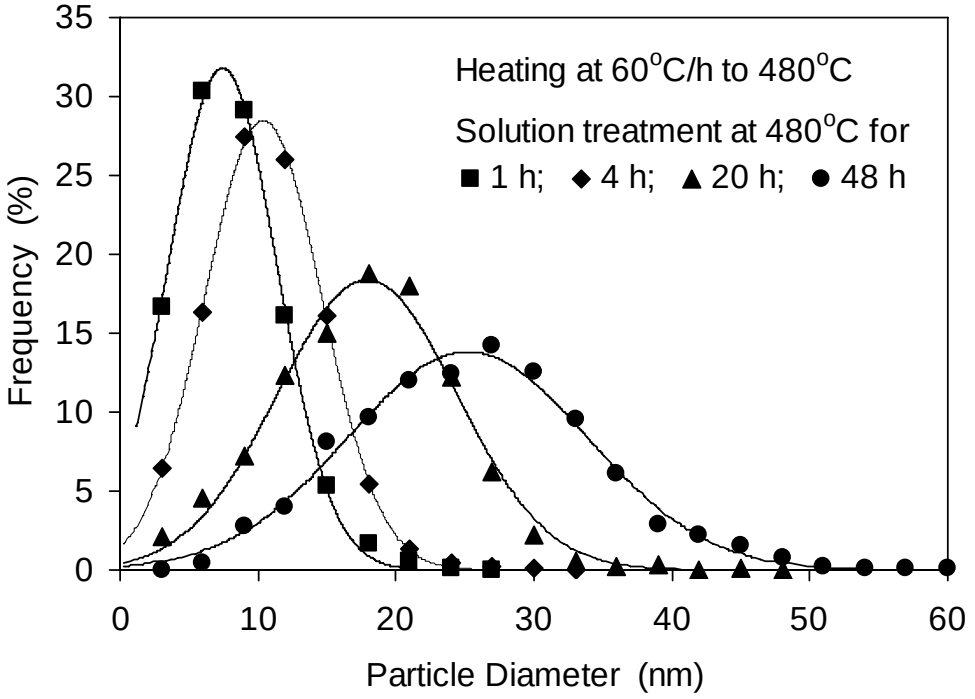
Heating at 60°C/h to 480°C
Solution treatment at 480°C for
1 h; 4 h; 20 h; 48 h
Frequency (%)
Particle Diameter (nm)
0
5
10
15
20
25
30
35
0
10
20
30
40
50
60

(b)

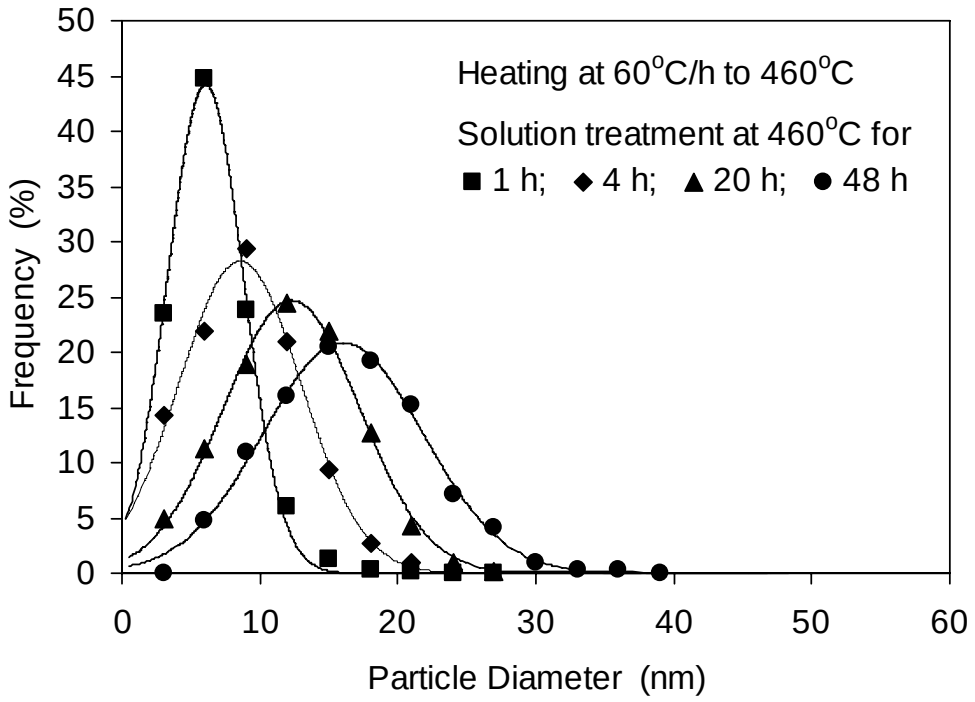

(c)

Figure 5. Size distributions of the $Al_3(Sc,Zr)$ particles in SSA018 alloy after different heat treatment: (a) heating from RT to 480ºC with a heating rate of 20ºC/h, holding at 480ºC for 1, 4, 20 and 48 hours; (b) heating from RT to 480ºC with a heating rate of 60ºC/h, holding at 480ºC for 1, 4, 20 and 48 hours; and (c) heating from RT to 460ºC with a heating rate of 60ºC/h, holding at 460ºC for 1, 4, 20 and 48 hours. The experimental data (solid symbols) are fitted by the normal distribution curves (solid lines).

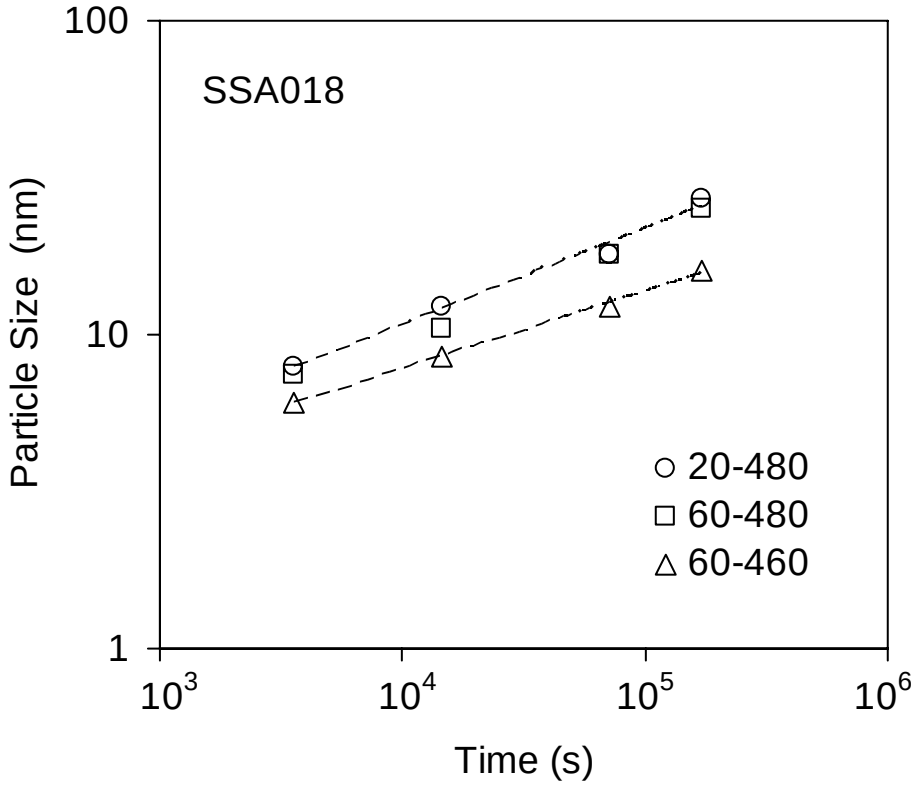

Figure 6. Mean size of $Al_3(Sc,Zr)$ particles in the DC cast SSA018 alloy versus solution treatment time at (○, □) 480°C and (Δ) 460°C. The specimens were heated to the temperatures with the heating rate of (○) 20ºC/h and (□, Δ) 60ºC/h.

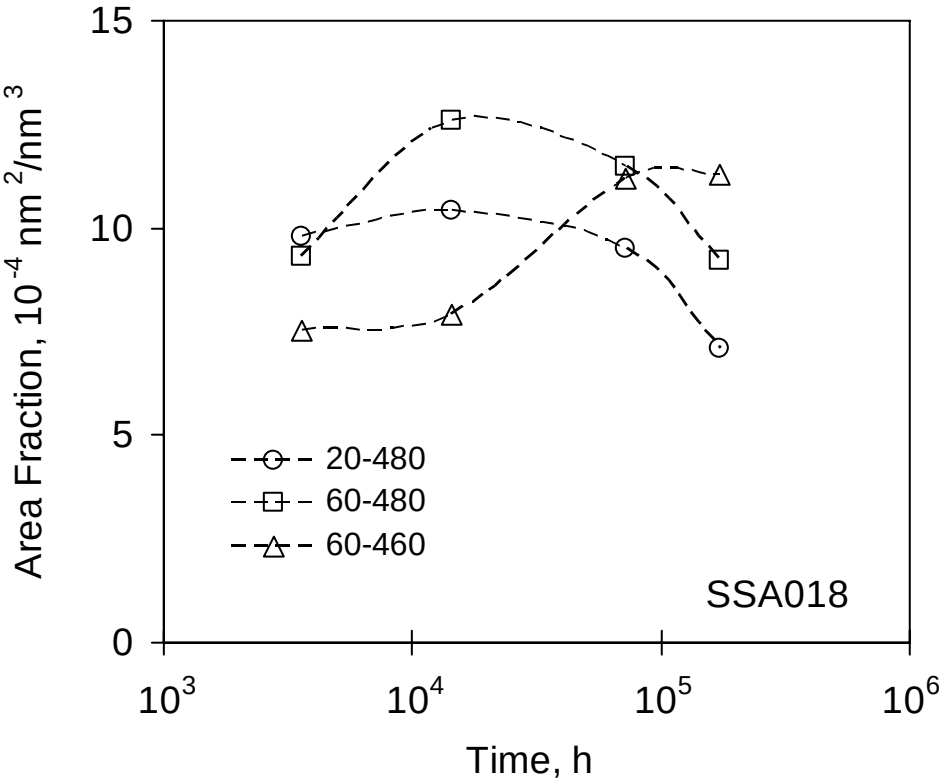

Figure 7. Surface area fraction of the $Al_3(Sc,Zr)$ particles versus solution treatment time at (○, □) 480°C and (Δ) 460°C. The specimens were heated to the temperatures with the heating rate of (○) 20ºC/h and (□, Δ) 60ºC/h.

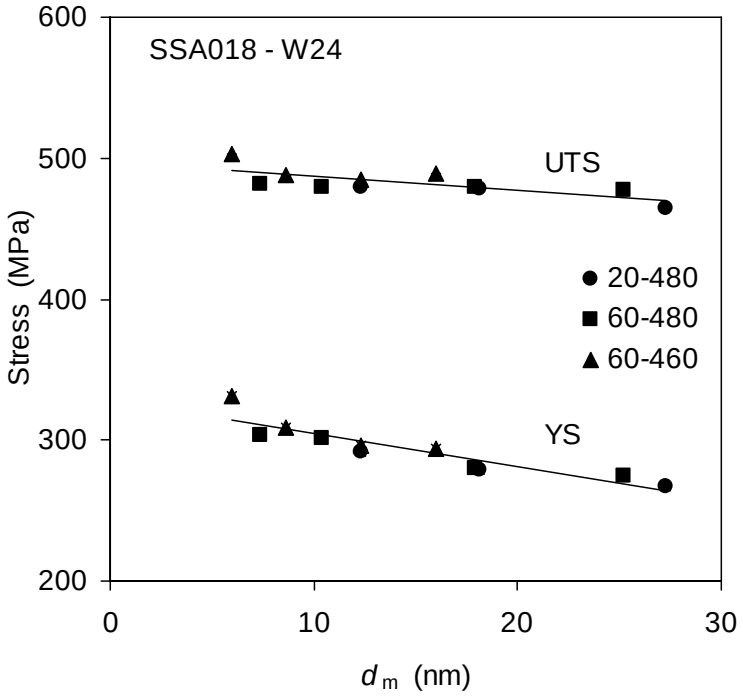

(a)

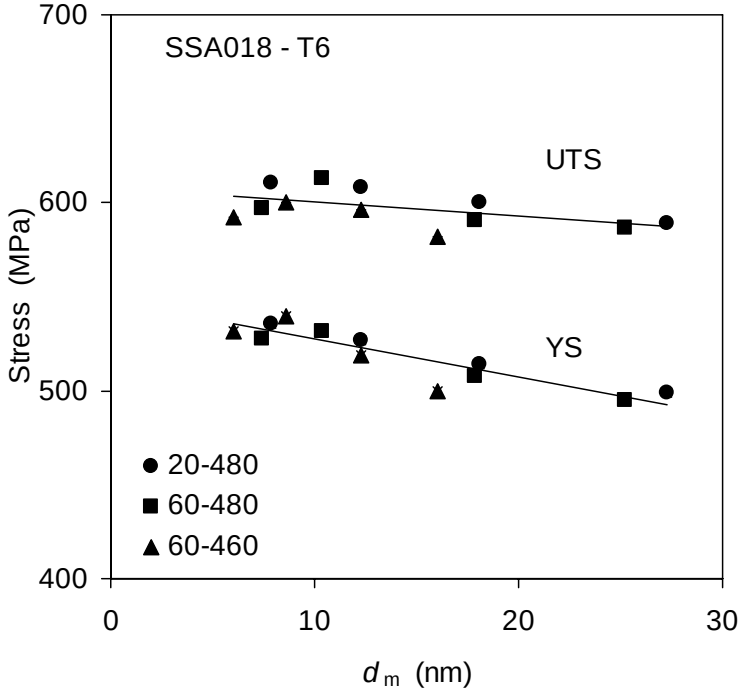

(b)

Figure 8. Dependence of the yield stress (YS) and ultimate tensile strength (UTS) on the mean diameter (d_m) of the $Al_3(Sc,Zr)$ particles in the SSA018 DC cast alloy after different solution treatments followed by (a) holding at room temperature for 24 hours (W24 temper) or (b) aging at 120ºC for 19 hours (T6 temper).

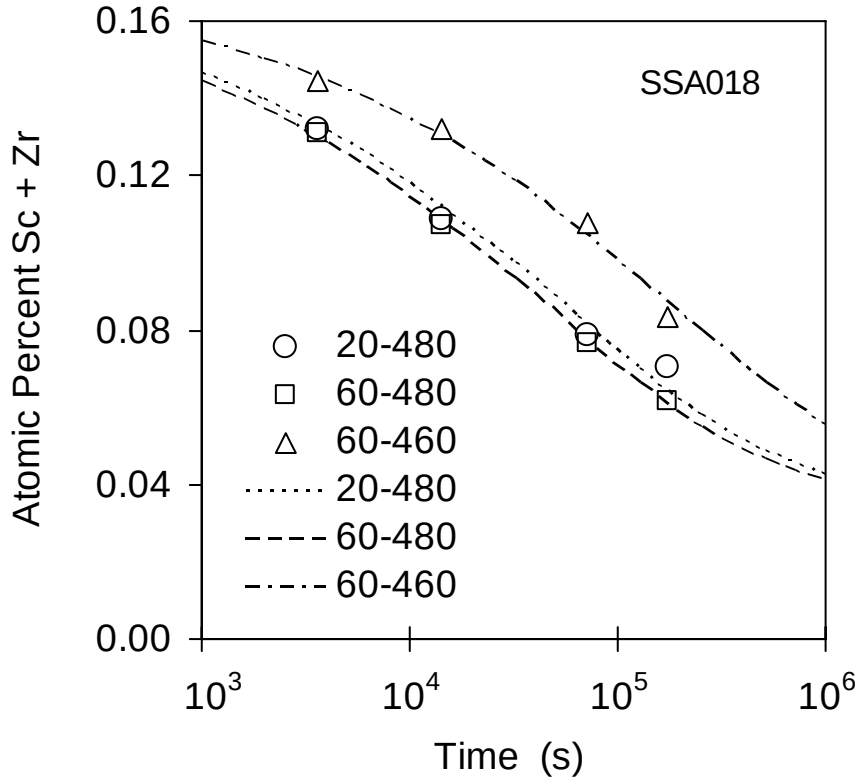

Figure 9. Concentrations of Sc+Zr in the aluminum matrix after different solution treatment times at (○, □) 480°C and (Δ) 460°C. The specimens were heated to the temperatures with the heating rates of (○) 20ºC/h and (□, Δ) 60ºC/h. The fitting lines correspond to the KJMA Equation (14) with the Avrami exponent $m = 0.404$ and the rate constant $K_3 = 1.20\text{x}10^{-2}$ s^{-m} (heat treatment 20-480), $1.31\text{x}10^{-2}$ s^{-m} (60-480), and $7.45\text{x}10^{-3}$ s^{-m} (60-460).

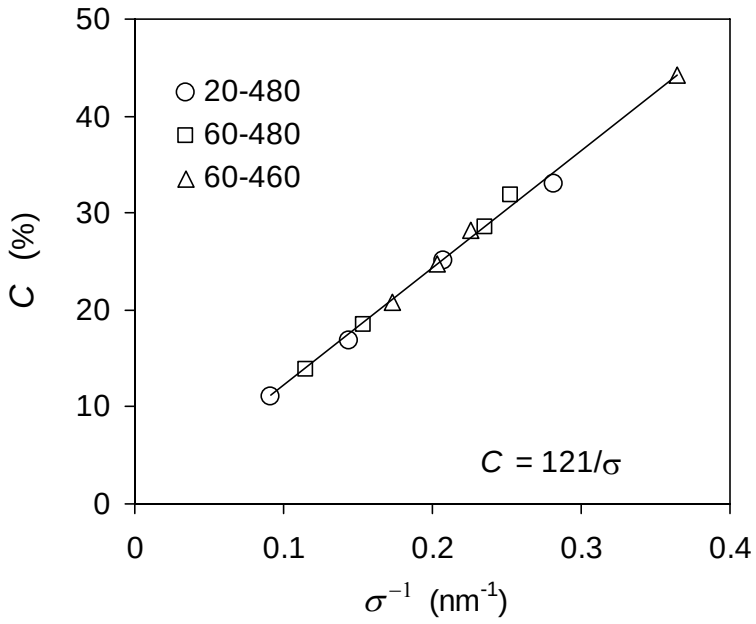

(a)

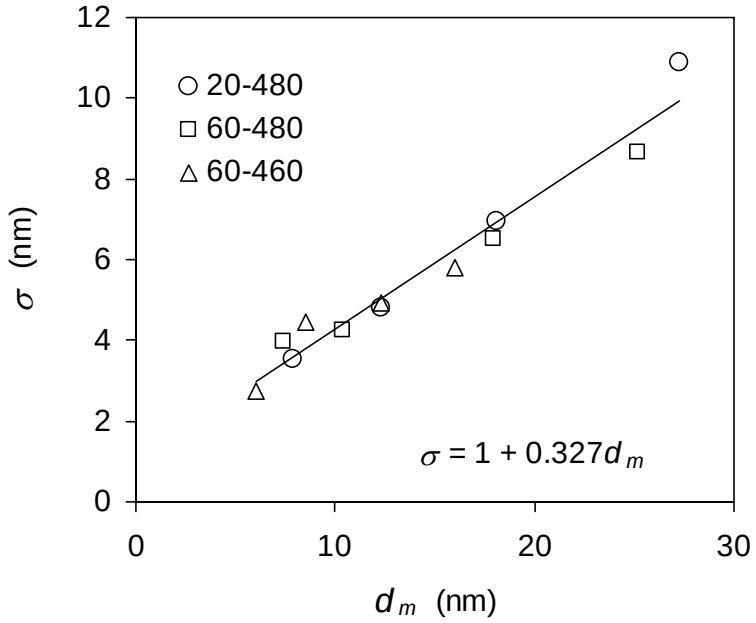

(b)

Figure 10. Relationships between parameters of Equation 1 describing size distributions of the $Al_3(Sc,Zr)$ particles after twelve different heat treatment conditions: (a) dependence of the standard deviation, σ, on mean particle diameter, d_m; (b) dependence of a pre-exponential term, C, on reciprocal of the standard deviation, σ^{-1}. Solid lines are linear fits with parameters given in the figures.

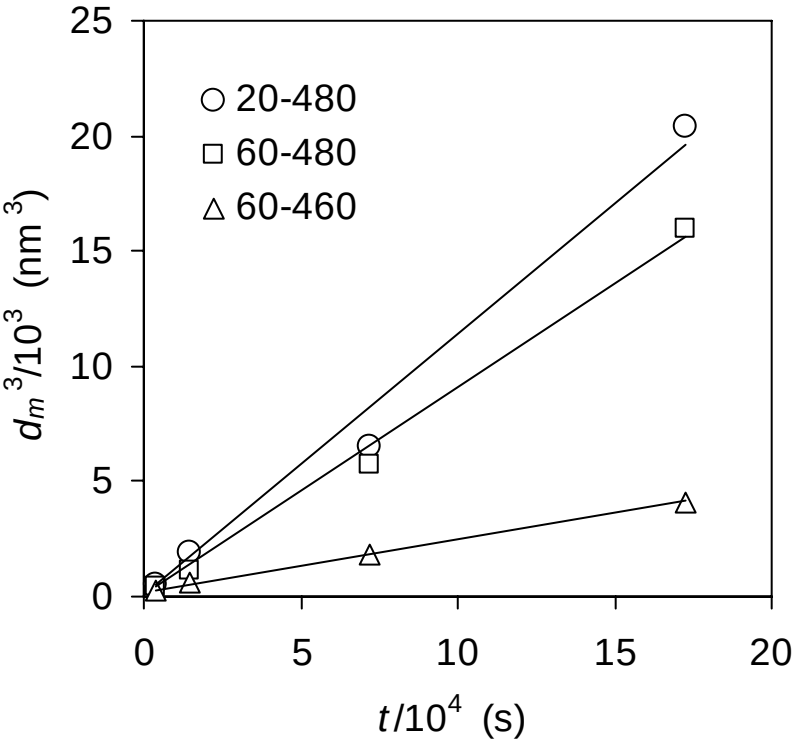

Figure 11. The mean $Al_3(Sc,Zr)$ particle size (open symbols) after different holding time at (○, □) 480°C and (Δ) 460°C plotted in coordinates $d_m{}^3$ vs. t. The specimens were heated to the temperatures with the heating rates of (○) 20ºC/h and (□, Δ) 60ºC/h. Solid lines correspond to linear fits of the experimental data by Equation (12). The initial particle size, d_{m0} (at $t = 0$) and the rate parameter K_2 as the fitting parameters, as well as the corresponding coefficient of determination, R^2, are given in Table 5.

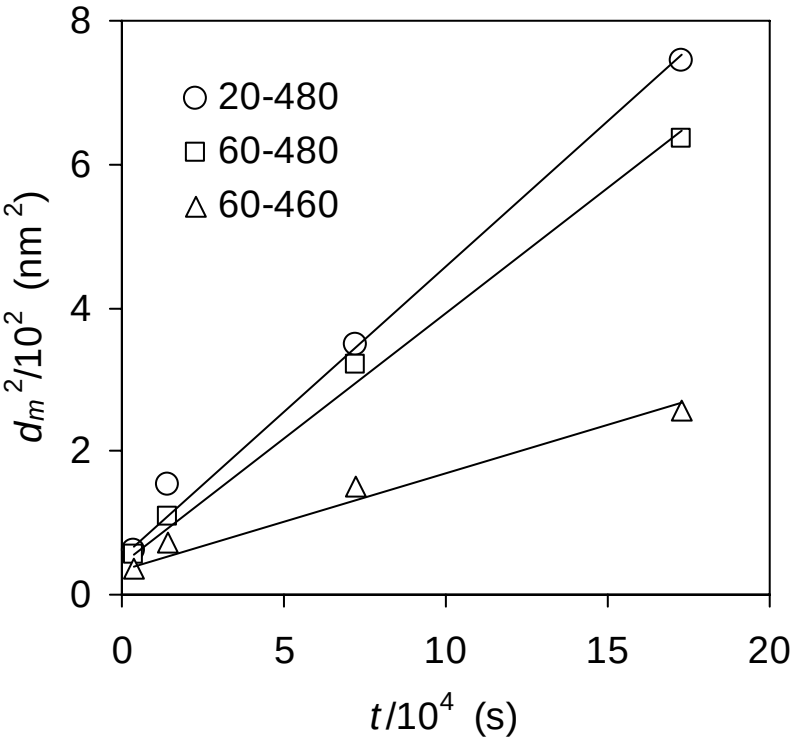

Figure 12. The mean $Al_3(Sc,Zr)$ particle size (open symbols) after different holding time at (○, □) 480°C and (Δ) 460°C plotted in coordinates d_m^2 vs. t. The specimens were heated to the temperatures with the heating rates of (○) 20ºC/h and (□, Δ) 60ºC/h. Solid lines correspond to linear fits of the experimental data by Equation (13). The initial particle size, d_{m0} (at $t = 0$) and the rate parameter K_2 as the fitting parameters, as well as the corresponding coefficient of determination, R^2, are given in Table 5.

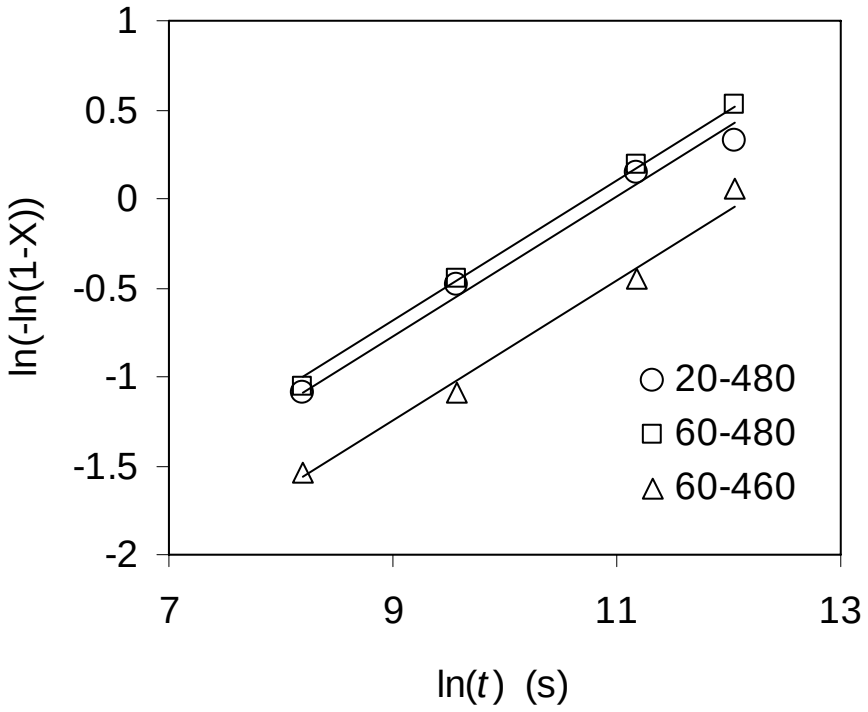

Figure 13. KJMA plot ln(-ln(1-*X*)) vs. ln(*t*) for the $Al_3(Sc,Zr)$ particle precipitation in the SSA018 alloy at (○, □) 480°C and (Δ) 460°C. The specimens were heated to the temperatures with the heating rates of (○) 20ºC/h and (□, Δ) 60ºC/h. The open symbols correspond to the experimental data and the fitting lines correspond to the KJMA Equation (14) with the Avrami exponent $m = 0.404$ and the rate constant $K_3 = 1.20\text{x}10^{-2}\ s^{-m}$ (heat treatment 20-480), $1.31\text{x}10^{-2}\ s^{-m}$ (60-480), and $7.45\text{x}10^{-3}\ s^{-m}$ (60-460).

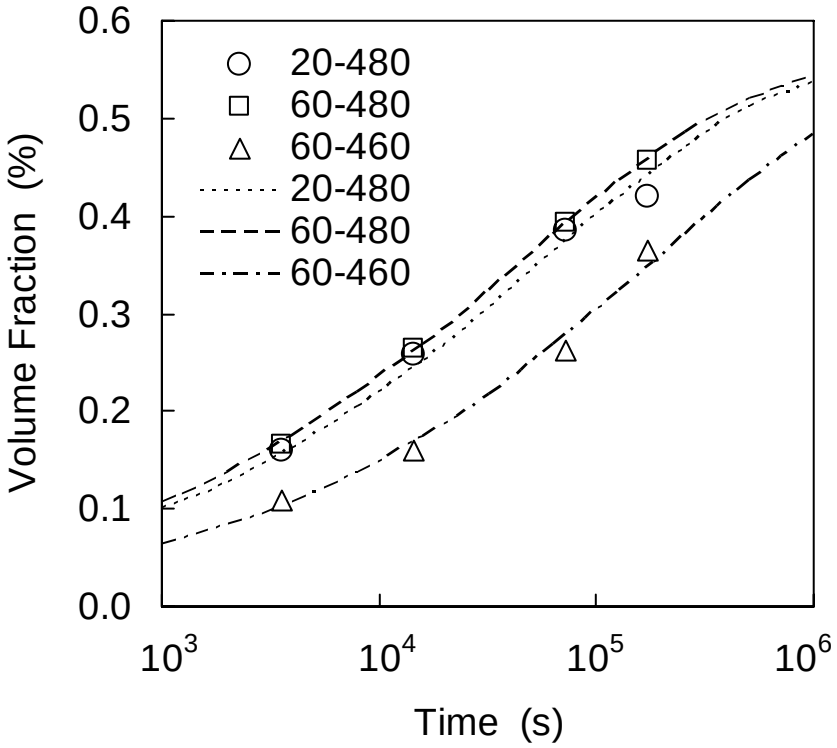

Figure 14. Dependence of the volume fraction of the $Al_3(Sc,Zr)$ particles on the solution treatment time at at (○, □) 480°C and (Δ) 460°C. The specimens were heated to the temperatures with the heating rates of (○) 20ºC/h and (□, Δ) 60ºC/h. The open symbols correspond to the experimental data and the fitting lines correspond to the KJMA Equation (14) with the Avrami exponent $m = 0.404$ and the rate constant $K_3 = 1.20\text{x}10^{-2}\ s^{-m}$ (heat treatment 20-480), $1.31\text{x}10^{-2}\ s^{-m}$ (60-480), and $7.45\text{x}10^{-3}\ s^{-m}$ (60-460).

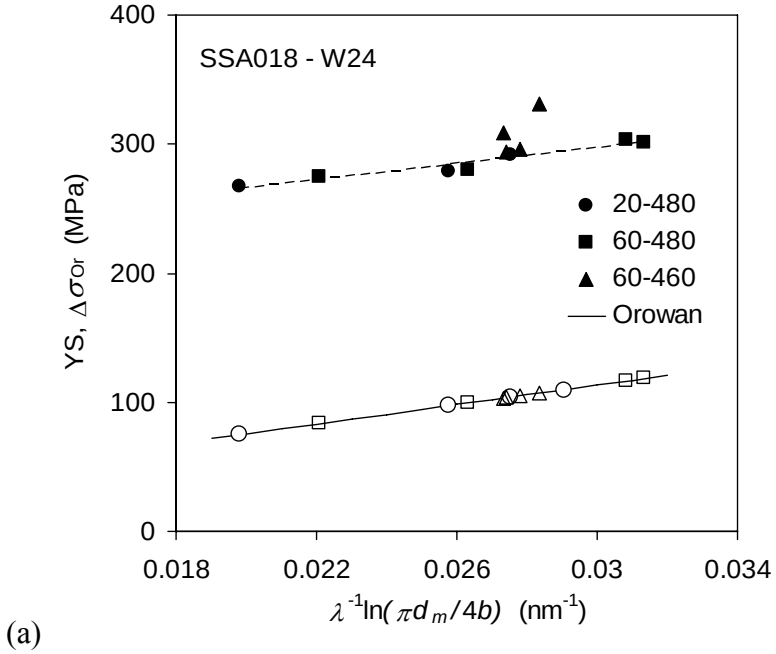

(a)

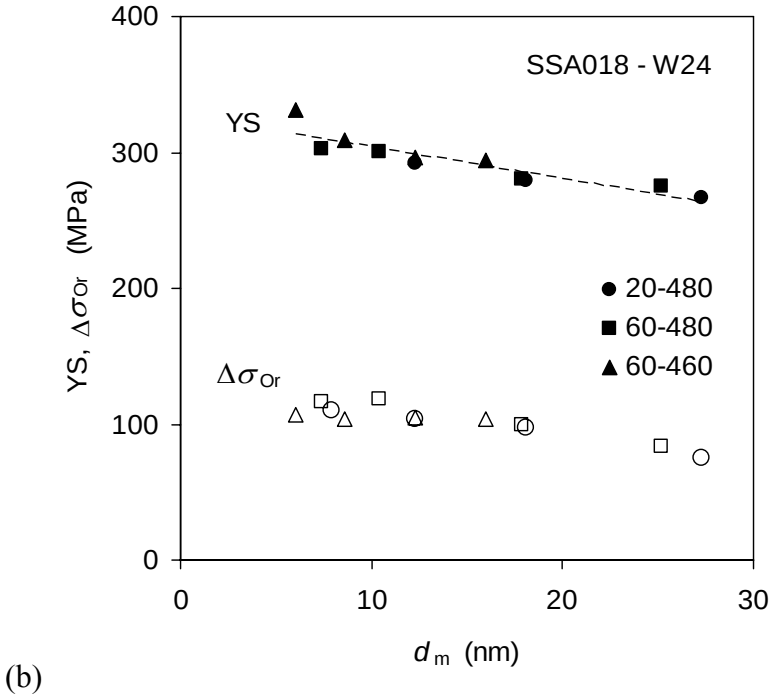

(b)

Figure 15. Dependence of the yield strength (YS) and Orowan strength ($\Delta\sigma_{Or}$) of the SSA018 alloy after W24 temper on (a) the inverse mean planar particle spacing (λ^{-1}, where $\lambda = \left[\frac{1}{2}\left(\frac{2\pi}{3f_V}\right)^{0.5} - 1\right]\frac{\pi d_m}{4}$) multiplied by the logarithm of the mean particle diameter (d_m) and (b) the mean particle diameter. Solid symbols are experimental data points and open symbols are calculated Orowan strength values corresponding to the experimental values of d_m and f_v for the $Al_3(Sc,Zr)$ particles from Table 2. A solid line in figure (a) corresponds to Equation 15 with the parameters given in the text. A dashed lines are the best fits of the experimental data points.

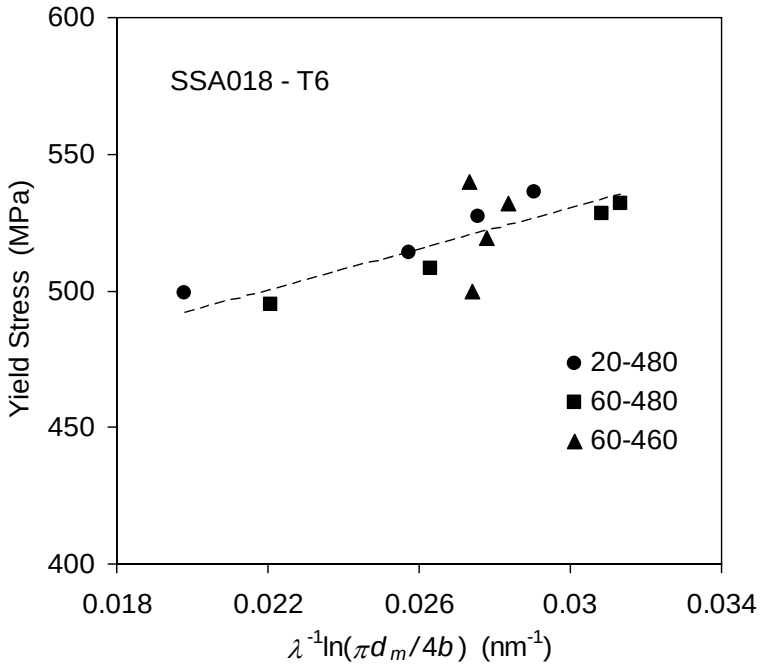

Figure 16. . Dependence of the yield stress of the SSA018 alloy after different solution treatments and aging at 120°C for 19 hours (T6 temper) on $\lambda^{-1}\ln(\pi d_m/4b)$ (where $\lambda = \left[\frac{1}{2}\left(\frac{2\pi}{3f_V}\right)^{0.5} - 1\right]\frac{\pi d_m}{4}$). The dashed line corresponds to Equation 17.